Solution Conformations of Potent Bicyclic Antagonists of Oxytocin by Nuclear Magnetic Resonance Spectroscopy and Molecular Dynamics Simulations

Mark D. Shenderovich, Katalin E. Kövér,† Susanne Wilke,‡ Nathan Collins,§ and Victor J. Hruby*

Contributed from the Department of Chemistry, University of Arizona, Tucson, Arizona 85721

Received October 28, 1996⊗

Abstract: The solution conformations of two potent bicyclic antagonists of oxytocin (H-Cys[1]-Tyr[2]-Ile[3]-Gln[4]-Asn[5]-Cys[6]-Pro[7]-Leu[8]-Gly[9]-NH_2, OT), [Mpa[1],*cyclo*(Glu[4],Lys[8])]OT, and [dPen[1], *cyclo*(Glu[4],Lys[8])]OT were studied by a combined use of ^{1}H and ^{13}C NMR spectroscopy in DMSO and molecular dynamics (MD) simulations. NMR data have suggested a model for the three-dimensional (3D) structure of the bicyclic analogues of OT (OT-BC) with a β-turn at the Tyr[2] and Ile[3] residues, and with a *cis* amide bond between Cys[6] and Pro[7]. A 3D structure containing a type III β-turn at Tyr[2]-Ile[3] has been shown to be consistent with NMR data. This structure was proposed as a model of the solution conformation of OT-BC and extensively tested by MD simulations with the AMBER force field. MD simulations at 300 K with NMR derived distance and φ torsion angle constraints demonstrated the consistency of this model with NMR data, and its stability was further demonstrated by non-constrained MD simulations. Dynamic properties of the 3D structure were explored by high-temperature MD at 500 K. Conformational transitions induced by a constrained rotation around the S−S bond revealed relatively low potential energy barriers (30 to 50 kJ/mol) between equilibrium left-handed and right-handed conformers of the disulfide bridge in OT-BC. A dynamic model of the solution structure of OT-BC with the relatively stable backbone conformation and a fast conformational equilibrium in the disulfide bridge and lactam bridge moieties was proposed as a result of the extensive MD simulations. The solution structure of OT-BC is consistent with structure−activity relations of peptide and non-peptide antagonists of OT. In particular, a β-turn at Tyr[2]-Ile[3] seems to be the common feature responsible for antagonist interaction with the uterine receptor of OT. On the other hand, the 3D structure of OT-BC differs considerably from the crystal and solution structures of OT analogues with agonist activity. Therefore, this study supports the hypothesis of different modes of receptor binding for agonists and antagonists of OT. The model of 3D structure of OT-BC proposed in this study may be used as a template for the rational design of peptide and non-peptide antagonists of oxytocin.

Introduction

Oxytocin, H-Cys-Tyr-Ile-Gln-Asn-Cys-Pro-Leu-Gly-NH_2 (OT), is a neurohypophyseal hormone physiologically important for its milk-ejecting and uterine-contracting activity in mammals. OT was the first peptide hormone whose primary structure was determined and proved by total synthesis.[1] Intensive structure−activity studies carried out for more than three decades have resulted in several hundred analogues of OT (see refs 2 and 3 for extensive reviews). The three-dimensional structure of oxytocin and the structurally related neurohypophyseal hormone vasopressin (VP) have been extensively investigated both by experimental and by theoretical methods (see refs 4 and 5 for reviews). Since the first model of solution conformation of OT was proposed by Urry and Walter,[6] several molecular mechanics[7] and molecular dynamics[8] studies have been aimed at determining low-energy conformations and at evaluating conformational mobility of neurohypophyseal hormones. Although a broad variety of models have been suggested for OT,[4−7] most researchers were in agreement that a conformation with a β-turn at positions 3 and 4, and with a reverse turn at positions 7 and 8, might be responsible for the uterotonic activity of OT and its analogues. This type of conformation was found also in the crystal structure of a potent OT agonist deaminooxytocin.[9]

* Author to whom correspondence should be addressed.

† Present address: L. Kossuth University, Department of Organic Chemistry, H-4010 Debrecen, P.O.B. 20, Hungary.

‡ Hoffmann-La Roche Inc., Medicinal Chemistry Bldg. 76, 340 Kingsland St., Nutley, NJ 07110.

§ Arris Pharmaceutical Corporation, 385 Oyster Point Blvd., Suite 3, South San Francisco, CA 94080.

⊗ Abstract published in *Advance ACS Abstracts,* June 1, 1997.

(1) du Vigneaud, V.; Ressler, C.; Swan, J. M.; Roberts, C. W.; Katsoyannis, P. G.; Gordon, S. *J. Am. Chem. Soc.* **1953**, *75*, 4879−4880.

(2) Jošt, K.; Lebl, M.; Brtnik, F., Eds. *CRC Handbook of Neurohypophyseal Hormone Analogs*; CRC Press: Boca Raton, FL, 1987; Vol. 2.

(3) Hruby, V. J.; Smith, C. W. In *Chemistry, Biology, and Medicine of Neurohypophyseal Hormones and Their Analogs*; Smith, C. W., Ed.; The Peptides: Analysis, Synthesis, Biology, Vol. 8; Academic Press: Orlando, 1987; pp 77−207.

(4) (a) Hruby, V. J.; Lebl, M. In *CRC Handbook of Neurohypophyseal Hormone Analogs*; Jošt, K., Lebl, M., Brtnik, F., Eds; CRS Press: Boca Raton, FL, 1987; Vol.1, Part 1, pp 105−155. (b) Malon, P. *Ibid*. pp 211−228.

(5) Hempel, J. C. In *Chemistry, Biology, and Medicine of Neurohypophyseal Hormones and Their Analogs*; Smith, C. W., Ed.; The Peptides: Analysis, Synthesis, Biology, Vol. 8, Academic Press: Orlando, 1987; pp 209−237.

(6) Urry, D. W.; Walter, R. *Proc. Natl. Acad. Sci. U.S.A.* **1971**, *68*, 956−958.

(7) (a) Kotelchuck, D.; Scheraga, H. A.; Walter, R. *Proc. Natl. Acad. Sci. U.S.A.* **1972**, *69*, 3629−3633. (b) DeCoen, J. L.; Ralston, E. *Biopolymers* **1977**, *16*, 1929−1943. (c) Nikiforovich, G. V.; Leonova, V. I.; Galaktionov, S. G.; Chipens, G. I. *Int. J. Pept. Protein Res.* **1979**, *13*, 363−373. (d) Spasov, V. Z.; Popov, E. M. *Sov. J. Bioorg. Chem.* **1981**, *7*, 263−273.

(8) (a) Hagler, A. T.; Dauber, P.; Osguthorpe, D. J.; Hempel, J. C. *Science* **1985**, *227*, 1309−1315. (b) Ward, D. J.; Chen, Y.; Platt, E.; Robson, B. *J. Theor. Biol.* **1991**, *148*, 193−227. (c) Bhaskaran, R.; Chang, L.-C.; Yu, C. *Biopolymers* **1992**, *32*, 1599−1608.

S0002-7863(96)03736-5 CCC: $14.00

Recent extensive electrostatically driven Monte Carlo simulations *in vacuo* and with a solvation-shell model have shown[10] that, despite restrictions imposed by the 20-membered disulfide ring, the OT molecule retains considerable conformational mobility, and energy preferences for several quite different types of conformations of OT are possible depending on the environment. This flexibility of the disulfide ring was probably the reason for different models of solution and receptor-bound conformations proposed for neurohypophyseal hormones in earlier studies.[6,7]

Inhibitors of the uterotonic activity of OT have been traditionally produced by introduction of bulky β-carbon substituents into position 1 and/or by substitution of L-tyrosine in position 2 of OT and VP with an aromatic D-amino acid.[11] Bulky β-carbon substituents in position 1 were shown to constrain the conformational mobility of the disulfide bridge moiety of OT and VP.[12] Nevertheless, both theoretical calculations and NMR studies showed[13,14] that substantial conformational mobility of the 20-membered disulfide ring was retained despite the additional conformational constraints imposed by substitutions in position 1.

A novel class of bicyclic antagonists of OT (OT-BC) has been prepared recently by amide bond cyclization between side chains in positions 4 and 8 of the amino acid sequence of a super-potent agonist deaminooxytocin ([Mpa^1]OT), which resulted in the primary structure:

$$\text{Xxx}^1\text{-Tyr}^2\text{-Ile}^3\text{-Glu}^4\text{-Asn}^5\text{-Cys}^6\text{-Pro}^7\text{-Lys}^8\text{-Gly}^9\text{-NH}_2$$

where Xxx is β'-mercaptopropionic acid ([Mpa^1]OT-BC, **1**)[15] or β'-mercapto-β,β-dimethylpropionic acid ([dPen^1]OT-BC, **2**).[16] Discovery of these potent, conformationally restrained antagonists with $pA_2 = 8.2$ and 8.74, respectively,[15,16] presents a unique opportunity to investigate conformational features responsible for the uterine receptor binding of oxytocin antagonists.

Schematic representation of the structure of OT-BC is shown in Figure 1. Extensive conformational analysis of OT-BC was first performed[17] with the ECEPP/2 force field,[18] using an elaborate build-up procedure. Low-energy conformations found for the bicyclic analogues were classified into several conformational families and compared to low-energy conformations of several monocyclic antagonists of OT with β-carbon substituents in position 1 of the disulfide ring. Three types of three-dimensional (3D) structure which showed a good overlap with the monocyclic antagonists were suggested as tentative models of binding conformations of OT-BC to the uterine receptor of OT.[17] These models differ mainly by the location of a type I or type III β-turn at residues 2,3 (Model 1), 3,4 (Model 2), or 4,5 (Model 3) of the disulfide ring (hereafter we define location of a β-turn by position numbers of its corner $i + 1$ and $i + 2$ residues). It also was shown[17] that the lactam bridge between Glu^4 and Lys^8 imposes severe constraints upon the configuration of the amide bond between Cys^6 and Pro^7. Only Model 3 allowed a *trans* conformation of this amide bond, while Models 1 and 2 favored a *cis* conformation. After the NMR studies of OT-BC were completed, the theoretically derived models were compared with NMR data obtained for [Mpa^1]OT-BC (**1**), and Model 1 was selected as a probable solution conformation of **1**.[19] This paper presents complete results[20] of NMR studies of two OT-BC analogues in DMSO and of extensive molecular dynamics refinement of their solution conformations based on the suggested tentative model.[17,19] A dynamic model of solution structure of two bicyclic analogues is proposed as a result of the combined NMR and MD studies, and structure−activity relationships of oxytocin antagonists are discussed in connection with the solution conformations of OT-BC.

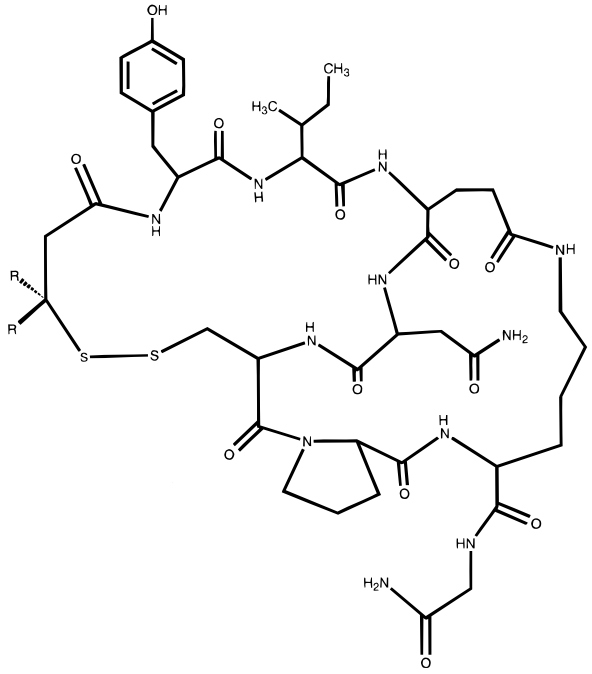

Figure 1. Structure of the bicyclic analogs of oxytocin. R = H and CH_3 for [Mpa^1]OT-BC and [dPen^1]OT-BC, respectively.

Experimental Procedures

The synthesis, characterization, and biological activity of the bicyclic analogues **1** and **2** have been published elsewhere.[15,16,21]

Nuclear Magnetic Resonance. All homo- and heteronuclear NMR experiments were carried out at 300 or 310 K with a Bruker AM-500

(9) Wood, S. P.; Tickle, I. J.; Treharne, A. M.; Pitts, J. E.; Mascarenhas, Y.; Li, J. Y.; Husain, J.; Cooper, S.; Blundell, T. L.; Hruby, V. J.; Buku, A.; Fishman, A.J.; Wyssbrod, H. R. *Science* **1986**, *232*, 633−636.

(10) Liwo, A.; Tempczyk, A.; Oldziej, S.; Shenderovich, M. D.; Hruby, V. J.; Talluri, S.; Ciarkowski, J.; Grzonka, Z. *Biopolymers* **1996**, *38*, 157−175.

(11) Lebl, M. In *CRC Handbook of Neurohypophyseal Hormone Analogs*; Jošt, K., Lebl, M., Brtnik, F., Eds.; CRS Press: Boca Raton, FL, 1987; Vol. 2, Part 1, pp 17−74.

(12) Tarnowska, M.; Liwo, A.; Shenderovich, M. D.; Liepina, I.; Golbraikh, A. A.; Grzonka, Z.; Tempczyk, A., *J. Comput.-Aided Mol. Des.* **1993**, *7*, 699−720.

(13) Shenderovich, M. D.; Kasprzykowski, F.; Liwo, A.; Sekacis, I.; Saulitis, J.; Nikiforovich, G. V. *Int. J. Pept. Protein Res.* **1991**, *38*, 528−538.

(14) Schmidt, J. M.; Ohlenschläger, O.; Rüterjans, H.; Grzonka, Z.; Kojro, E.; Pavo I.; Fahrenholz, F. *Eur. J. Biochem.* **1991**, *201*, 355−371.

(15) Hill, P. S.; Smith, D. D.; Slaninova, J.; Hruby, V. J. *J. Am. Chem. Soc.* **1990**, *112*, 3110−3113.

(16) Smith, D. D.; Slaninova, J.; Hruby, V. J. *J. Med. Chem.* **1992**, *35*, 1558−1563.

(17) Shenderovich, M.; Balodis, J.; Mishlyakova, N.; Liwo, A.; Kasprzykowski, F.; Kasprzykowska, R.; Tarnowska, M.; Ciarkowski, J. In *Peptides 1992. Proceedings of the 22nd European Peptide Symposium*; Schneider, C. H., Eberle, A. N., Eds.; ESCOM: Leiden, 1993; pp 535−536.

(18) (a) Momany, F. A.; McGuire, R. F.; Burgess, A. W.; Scheraga, H. A. *J. Phys. Chem.* **1975**, *79*, 2361−2381. (b) Némethy, G.; Pottle, M. S.; Scheraga, H. A. *J. Phys. Chem.* **1983**, *87*, 1883−1887.

(19) Shenderovich, M.; Wilke, S.; Kövér, K.; Collins, N.; Hruby, V.; Liwo, A.; Ciarkowski, J. *Polish J. Chem.* **1994**, *68*, 921−927.

(20) For a brief preliminary communication on this study see: Shenderovich, M. D.; Kövér, K. E.; Wilke, S.; Romanowski, M.; Liwo, A.; Lankiewich, L.; Gwizdala, E.; Ciarkowski, J.; Hruby, V. J. In *Peptides: Chemistry, Structure and Biology; Proceedings of the 14th American Peptide Symposium*; Kaumaya, P. T. P., Hodges, R. S., Eds.; Mayflower Scientific Ltd.: England, 1996; pp 499−500.

(21) Hruby, V. J.; Wilke, S.; Al-Obeidi, F.; Jiao, D.; Lin, Y. *Reactive Polymers* **1994**, *22*, 231−241.

spectrometer (500 MHz proton and 125 MHz carbon frequency) equipped with an ASPECT-3000 computer and a 5-mm multinuclear inverse probehead. Data processing and analyses were done using either Bruker software or *Felix* software[22] on a Silicon Graphics Iris workstation. Peptides **1** and **2** were analytically pure by HPLC and TLC analysis. The samples were extensively dried *in vacuo* to remove residual water. Deuterated solvent was purchased from ISOTECH, Inc. as dimethyl-d_6 sulfoxide "100%'' (DMSO-d_6). **1** (18 mg) or 30 mg of **2** was dissolved in 0.5 mL of DMSO-d_6. Chemical shifts were calibrated to the DMSO-d_6 solvent signal at 2.49 ppm for ^{1}H and 39.5 ppm for ^{13}C.

Proton resonance assignments[23] were achieved by the combined use of 2D total correlated spectroscopy (TOCSY),[24] particularly *z*-filtered TOCSY,[25] and dipolar correlated 2D nuclear Overhauser enhancement spectroscopy (NOESY).[26] All proton spin systems of individual amino acid residues were identified with the use of TOCSY spectra, whereas the sequential resonance assignment relied on the detection of inter-residue dipolar interactions between $C^{\alpha}H_i$ and NH_{i+1} protons, and/or between NH_i and NH_{i+1} protons with 2D NOESY experiments.[23] Figure 2 shows the expanded fingerprints of NH/NH (a) and NH/aliphatic CH (b) regions of the NOESY spectrum for [dPen^1]OT-BC (**2**). The *z*-filtered TOCSY spectrum of **2** is included in the Supporting Information.

^{1}H-NMR data, including chemical shifts and coupling constants, reported in Tables 1 and 2, respectively, were extracted from the resolution-enhanced 1D spectra in combination with the highly digitized 1D traces of *z*-filtered TOCSY spectra. Five 1D proton spectra were recorded at 5-deg intervals from 298 to 318 K to measure temperature coefficients $\Delta\delta/\Delta T$ for amide protons, which are included in Table 1. The coupling constants $^3J_{NH\alpha}$ were used to estimate the φ torsion angles for corresponding residues according to the modified Karplus equation.[27] The coupling constants $^3J_{\alpha\beta}$ in combination with the observed intraresidue NH−H$^{\beta}$ and H$^{\alpha}$−H$^{\beta}$ NOEs were used where possible for the stereospecific assignment of $C^{\beta}H_2$ protons[28] (see Table 1) and for determination of side chain rotamer populations[29] given in Table 2. In particular, the pattern observed for the high-field β-protons of Tyr^2, Asn^5, and Cys^6 in **2** and of Lys^8 in **1** and **2**, which show NOEs with NH and large couplings with H$^{\alpha}$, is characteristic of the *pro-R* H$^{\beta}$, and suggests a predominance of the *gauche (−)* rotamers of these side chains (Tables 1 and 2).

NOESY spectra were recorded at 310 K with different mixing times τ_m = 75, 100, 200, 300, and 400 ms in order to check for the initial linearity of the nuclear Overhauser enhancement (NOE) build up and for the impact of spin diffusion.[26] NOEs observed at the mixing times of 75 and 100 ms were unaffected by spin diffusion, and NOE intensities were classified as strong (s), medium (m), and weak (w) according to the number of contours in cross peaks of NOESY spectra recorded with τ_m = 100 ms.

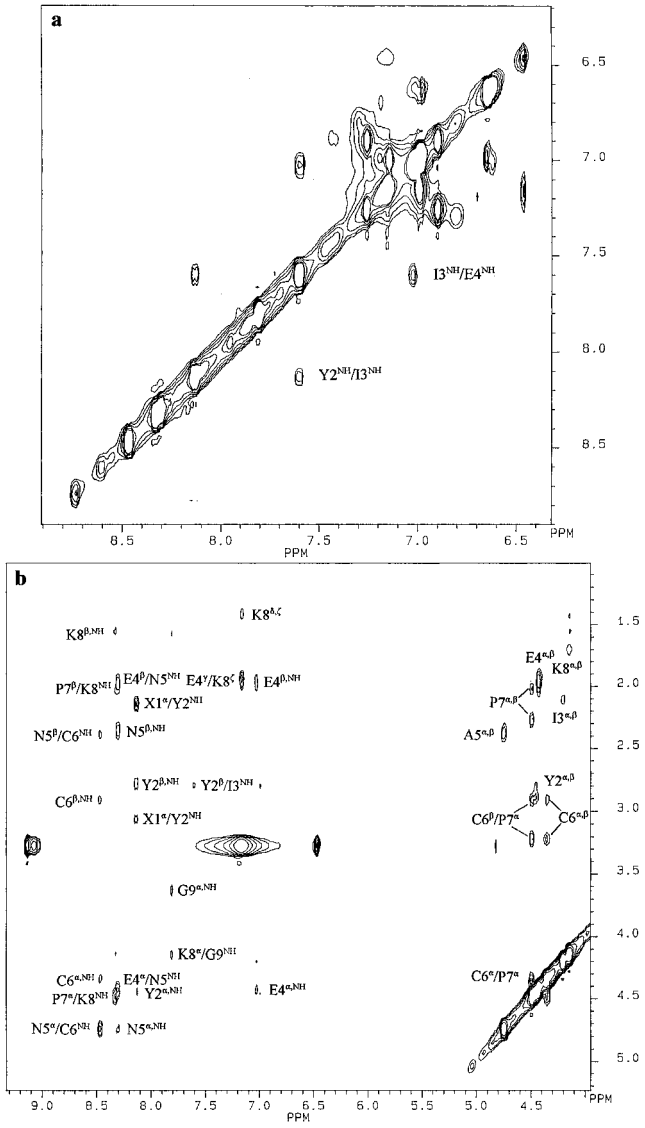

Figure 2. Expanded fingerprints of NH/NH (a) and NH/aliphatic CH (b) regions of the NOESY spectrum of [dPen^1]OT-BC measured in DMSO-d_6 at 310 K with the mixing time of 100 ms.

Proton detected heteronuclear correlation spectroscopy, including multiplet-edited HSQC[30] and carbon-coupled HMQC-TOCSY[31,32] experiments, was used for the assignment of protonated carbon resonances, as well as to resolve the ambiguities in the proton resonance assignment. Due to the phase-edited nature of the HSQC spectrum, the origin of correlations from either methylene or methine/methyl groups, observed at the respective carbon chemical shift, could easily be determined. In the carbon-coupled HMQC-TOCSY spectrum, the distinctly different multiplet structures of one-bond (direct) and relay correlations, namely the direct correlations with characteristic large splitting due to $^1J_{CH}$, allowed an unambiguous assignment of all resonances. ^{13}C chemical shifts of protonated carbons are given in Table 3. The double-INEPT-type HSQC inverse heteronuclear correlation sequence[33] was used for ^{13}C T_1 measurements on analogue **1**. The experimental parameters used for the NMR measurements are given in the Supporting Information.

(22) *Felix User Guide, Version 2.3*, Biosym Technologies, San Diego, CA, 1993.

(23) Wüthrich, K. *NMR of Proteins and Nucleic Acids*, John Wiley; New York, 1986.

(24) (a) Braunschweiler, L.; Ernst, R. R. *J. Magn. Reson.* **1983**, *53*, 521−528. (b) Bax, A.; Davis, D. G. *J. Magn. Reson.* **1985**, *63*, 207−213. (c) Davis, D. G.; Bax, A. *J. Am. Chem. Soc.* **1985**, *107*, 2820−2821.

(25) (a) Subramanian, S.; Bax, A. *J. Magn. Reson.* **1987**, *71*, 325−330. (b) Rance, M. *J. Magn. Reson.* **1987**, *74*, 557−564.

(26) (a) Noggle, J. H.; Schirmer, R. E. *The Nuclear Overhauser Effect, Chemical Applications*; Academic Press: New York, 1971. (b) Jeener, J.; Meier, B. H.; Bachmann, P.; Ernst, R. R. *J. Chem. Phys.* **1979**, *71*, 4546−4553. (c) Kumar, A.; Ernst, R. R.; Wüthrich, K. *Biochem. Biophys. Res. Commun.* **1980**, *95*, 1−6. (d) Neuhaus, D.; Williamson, M. P. *The Nuclear Overhauser Effect*; VCH: Weinheim, 1989.

(27) (a) Karplus, M. J. *J. Am. Chem. Soc.* **1963**, *85*, 2870−2871. (b) Bystrov, V. F. In *Progress in Nuclear Magnetic Resonance Spectroscopy*; Emsley, J. W., Feeney, J., Sutcliffe, L. H., Eds.; Pergamon Press: Oxford, 1976; Vol. 10, pp 41−81.

(28) (a) Wagner, G.; Braun, W.; Go, N.; Havel, T. F.; Schaumann, T.; Wüthrich, K. *J. Mol. Biol.* **1987**, *196*, 611−638. (b) Arseniev, A.; Schultze, P.; Wörgötter, E.; Braun, W.; Wagner, G.; Vasak, M.; Kagi, J. H. R.; Wüthrich, K. *J. Mol. Biol.* **1988**, *201*, 637−657. (c) Zuiderweg, E. R. P.; Boelens, R.; Kaptein, R. *Biopolymers* **1985**, *24*, 601−611.

(29) (a) Pachler, K. G. R. *Spectrochim. Acta* **1963**, *19*, 2085−2092; (b) Pachler, K. G. R. *Spectrochim. Acta* **1964**, *20*, 581−587. (c) Cung, M. T.; Marraud, M. *Biopolymers* **1982**, *21*, 953−967. (d) Hansen, P. E.; Feeney, J.; Roberts, G. C. K. *J. Magn. Reson.* **1975**, *17*, 249−261.

(30) (a) Davis, D. G. *J. Magn. Reson.* **1991**, *91*, 665−672. (b) Kövér, K. E.; Prakash, O.; Hruby, V. J. *Magn. Reson. Chem.* **1993**, *31*, 231−237.

(31) (a) Lerner, L.; Bax, A. *J. Magn. Reson.* **1986**, *69*, 375−380. (b) Davis, D. G. *J. Magn. Reson.* **1989**, *84*, 417−424. (c) Kövér, K. E.; Prakash, O.; Hruby, V. J. *J. Magn. Reson.* **1992**, *99*, 426−432.

(32) Bax, A.; Davis, D. G. *J. Magn. Reson.* **1985,** *65*, 355−360.

(33) (a) Nirmala, N. R.; Wagner, G. *J. Am. Chem. Soc.* **1988**, *110*, 7557−7558. (b) Kay, L. E.; Nicholson, L. K.; Delaglio, F.; Bax, A.; Torchia, D. A. *J. Magn. Reson.* **1992**, *97*, 359−375.

Table 1. ^{1}H Chemical Shifts[a] and NH Temperature Coefficients[b] of [Mpa^1]OT-BC (**1**) and [dPen^1] OT-BC (**2**) Analogues

residue		NH[b]	H^{α}	$H^{\beta 1}$ [d]	$H^{\beta 2}$ [d]	others[b]
Xxx^1	**1**		2.66, 2.38	2.97	2.77	
	2		3.06, 2.13			$CH_3{}^{\gamma 1}$ 1.46, $CH_3{}^{\gamma 2}$ 0.97
Tyr^2	**1**	8.14 (4.4)	4.35	2.86[c]		H^{Ar} 6.68, 6.95
	2	8.14 (5.1)	4.45	2.89 (*pro-S*)	2.77 (*pro-R*)	H^{Ar} 6.67, 6.99
Ile^3	**1**	7.88 (2.3)	4.05	2.06		$H^{\gamma 1}$ 1.28, $H^{\gamma 2}$ 1.08, $CH_3{}^{\gamma}$ 0.82, $CH_3{}^{\delta}$ 0.84
	2	7.60 (0.15)	4.20	2.11		$H^{\gamma 1}$ 1.27, $H^{\gamma 2}$ 1.11, $CH_3{}^{\gamma}$ 0.83, $CH_3{}^{\delta}$ 0.85
Glu^4	**1**	7.09 (0.5)	4.40	1.8−2.0		$H^{\gamma 1,\gamma 2}$ 1.8−2.0
	2	7.02 (0.35)	4.42	1.9−2.0		$H^{\gamma 1,\gamma 2}$ 1.9−2.0
Asn^5	**1**	8.31 (7.2)	4.64	2.37	2.35	
	2	8.31 (5.7)	4.74	2.39 (*pro-S*)	2.33 (*pro-R*)	
Cys^6	**1**	8.36 (8.8)	4.40	3.14 (*pro-S*)	2.97 (*pro-R*)	
	2	8.49 (10.0)	4.34	3.22 (*pro-S*)	2.90 (*pro-R*)	
Pro^7	**1**		4.50	2.26	2.00	$H^{\gamma 1,\gamma 2}$ 1.74, $H^{\delta 1}$ 3.45, $H^{\delta 2}$ 3.35
	2		4.48	2.27	2.02	$H^{\gamma 1,\gamma 2}$ 1.74, $H^{\delta 1}$ 3.43, $H^{\delta 2}$ 3.34
Lys^8	**1**	8.32 (7.2)	4.14	1.69 (*pro-S*)	1.55 (*pro-R*)	$H^{\gamma 1}$ 1.44, $H^{\gamma 2}$ 1.40, $H^{\delta 1,\delta 2}$ 1.39 $H^{\epsilon 1}$ 3.13, $H^{\epsilon 2}$ 3.10, NH^{ζ} 7.25 (4.4)
	2	8.34 (5.5)	4.14	1.71 (*pro-S*)	1.55 (*pro-R*)	$H^{\gamma 1,\gamma 2,\delta 1,\delta 2}$ 1.34−1.45 $H^{\epsilon 1}$ 3.19, $H^{\epsilon 2}$ 2.99, NH^{ζ} 7.16 (2.4)
Gly^9	**1**	7.82 (8.4)	3.62[c]			
	2	7.82 (8.0)	3.62[c]			

[a] Obtained in DMSO-d_6 at 300 K. Chemical shifts were referenced to the residual DMSO solvent signal at 2.49 ppm. [b] $\Delta\delta/\Delta T$ in DMSO-d_6 are given in parentheses (in ppb/K). [c] Chemically equivalent geminal protons. [d] Diastereotropic assignment of H^{β} is given in parentheses.

Table 2. Proton Vicinal Coupling Constants and Side Chain Rotamer Populations for [Mpa^1]OT-BC (**1**) and [dPen^1]OT-BC (**2**) in DMSO at 300 K

	vicinal coupling constants, Hz				χ^1 rotamer populations, %[b]					
	$^3J_{NH\alpha}$		$^3J_{\alpha\beta}$[a]		**1**			**2**		
residue	**1**	**2**	**1**	**2**	g^-	t	g^+	g^-	t	g^+
Xxx^1			13.7, 5.5							
Tyr^2	8.9	9.6	8.2[d]	5.4, 10.5			12	64	18	18
Ile^3	8.9	9.9	5.5	4.6	26			18		
Glu^4	7.1	7.1	4.4[d]	3.7[d]			67			80
Asn^5	6.9	6.7	5.5, 8.9	4.5, 9.7	58[e]	26[e]	16	65	17	18
Cys^6	8.2	8.1	0−1,[c] 8.2	0−1,[c] 11.3	≈50	0	≈50	≈80	0	≈20
Pro^7			8.9, 0−1[c]	6.3, 0−1[c]						
Lys^8	8.2	7.7	4.1, 7.5	3.7, 10.4	45	14	41	71	10	19
Glu^9	6.2	6.0								

[a] $^3J_{\alpha\beta}$ of the low-field protons are listed first. [b] Rotamer populations were calculated from $^3J_{\alpha\beta}$ as described in the Experimental Section. [c] These coupling constants could not be measured even with a final digital resolution of 0.3 Hz/point. [d] For degenerate or overlapping $C^{\beta}H_2$ resonances the sum of two $^3J_{\alpha\beta}$ constants was determined from the H^{α} multiplets. Average values of two $^3J_{\alpha\beta}$ are given in the Table. Populations of g^+ rotamers were estimated from the sum of two $^3J_{\alpha\beta}$.[29d] [e] Assignment of g^- and t rotamers is arbitrary.

Molecular Dynamics Simulations. Energy minimization and molecular dynamics (MD) simulations were performed with the AMBER* force field[34] implemented in the MacroModel BatchMin Version 3.1 on a CONVEX C220 computer system. Visualization and manipulation with molecules were carried out on Silicon Graphics Iris workstations with use of the interactive MacroModel program[35] (versions 4.0 and 4.5).

Table 3. ^{13}C Chemical Shifts[a] of [Mpa^1]OT-BC (**1**) and [dPen^1] OT-BC (**2**) Analogues

residue		C^{α}	C^{β}	C^{γ}	C^{δ}	C^{ϵ}	C^{Ar}
Xxx^1	**1**	35.9	32.3				
	2	47.5		25.7, 27.9			
Tyr^2	**1**	56.7	37.1				129.9, 115.4
	2	56.2	37.0				130.1, 115.2
Ile^3	**1**	57.7	35.5	24.0 (CH_2)	16.5		
				16.1 (CH_3)			
	2	57.2	36.3	24.5 (CH_2)	11.9		
				16.4 (CH_3)			
Glu^4	**1**	50.4	31.0	30.9			
	2	50.8	31.0	31.0			
Asn^5	**1**	50.4	37.1				
	2	50.5	37.5				
Cys^6	**1**	49.7	43.8				
	2	49.8	45.1				
Pro^7	**1**	58.7	31.8	21.7	47.2		
	2	58.9	32.3	22.3	47.3		
Lys^8	**1**	53.0	31.2	23.8	28.4	38.5	
	2	53.5	31.4	24.0	28.9	39.0	
Gly^9	**1**	41.8					
	2	42.2					

[a] Obtained in DMSO-d_6 at 310 K. Chemical shifts were referenced to the DMSO-d_6 solvent signal at 39.5 ppm.

All MD simulations employed the Verlet velocity integration algorithm[36] with a 0.5 fs time step. Simulations at 300 K were started with a 50 ps equilibration run and followed by a 100 ps acquisition run, while simulations at 500 K generally were started with 10 ps thermalization followed by 50 ps equilibration and 200 ps acquisition

(34) (a) Weiner, S. J.; Kollman, P. A.; Case, D. A.; Chandra Singh, U.; Ghio, C.; Alagona, G.; Profeta, S.; Weiner, P. *J. Am. Chem. Soc.* **1984**, *106*, 765−784. (b) Weiner, S. J.; Kollman, P. A.; Nguyen, D. T.; Case, D. A. *J. Comput. Chem.* **1986,** *7*, 230−252.

(35) (a) Mohamadi, F.; Richards, N. G. J.; Guida, W. C.; Liskamp, R.; Lipton, M.; Caufield, C.; Chang, G.; Hendrickson, T.; Still W. K. *J. Comput. Chem.* 1990, *11*, 440−467. (b) *MacroModel; Interacrive Molecular Modeling System, Version 4.5*; Department of Chemistry, Columbia University; New York, 1994.

(36) Verlet, L. *Phys. Rew.* **1967**, *159*, 98−103.

runs. One hundred structures saved from each MD trajectory in equal time steps were used to calculate average characteristics of MD trajectories. Conformations stored during selected MD trajectories were energy minimized with the Polak-Ribiere conjugated gradient algorithm[37] to a gradient less than 0.05 kJ/(Å·mol). Solvent effects were not included into calculations explicitly. In order to account in part for the DMSO solvent and to avoid overweighting of compact, internally hydrogen-bonded conformations, the dielectric constant $\epsilon = 45$ was used in all calculations. All hydrogen atoms were explicitly included into calculations, covalent bonds to hydrogens being kept fixed by the SHAKE algorithm.[38]

The following MD simulations were performed for [Mpa^1]OT-BC: (1) free (nonrestrained) MD at 300 K (FMD); (2) distance-restrained MD at 300 K (DMD) including interproton distance constraints derived from NOE data; (3) torsion-angle-restrained MD at 300 K (TMD), which constrained φ torsion angles around the values derived from experimental $^3J_{NH\alpha}$ coupling constants; and (4) free MD at 500 K (MD500). Free simulations at 300 and 500 K and distance-restrained MD simulations at 300 K were performed also for [dPen^1]OT-BC. MD simulations at 300 K were performed for two initial conformations obtained in our preliminary study,[19] which represented Model 1 of the 3D structure[17] of OT-BC with the left-handed and right-handed conformations of the disulfide bridge. The initial conformations were energy minimized at the conditions of each MD run. Several low-energy conformations of each molecule found in MD simulations at 300 K were used as initial structures for simulations at 500 K.

Distance constraints were incorporated in MD simulations as harmonic potentials $U_{dr} = U_o(r - r_o)^2$, while cosine potentials $U_{tr} = U_o \cos(\phi - \phi_o)^2$ were used as torsion angle constraints. No penalty potentials were applied within flat-bottom wells $r_o \pm \Delta r$ and $\phi_o \pm \Delta\phi$. Force constants U_o for penalty potentials and widths of the flat-bottom wells were selected depending on relative NOE intensities and aims of particular simulations (see Results and Discussion).

In order to induce conformational transitions around the disulfide bond, strong cosine penalty potentials ($U_o = 1000$ kJ/mol) were applied to constrain the torsion angle χ_{SS}(C$^\beta$−S−S−C$^\beta$) within a flat-bottom window $\chi^0_{SS} \pm 10°$, and the center χ^0_{SS} of the window was moved with a 20° step between two equilibrium values at ±90° over the energy barriers at $\chi_{SS} = 180°$. Two protocols were used to allow relaxation of all degrees of freedom of the molecule in each χ_{SS} window. In the first protocol, a restrained minimization of potential energy of the molecule was performed in each consecutive χ_{SS} window. In the second protocol, continuous MD simulations at 300 K were performed in the consecutive windows, the χ_{SS} constraints being shifted each 5 or 10 ps, and final MD structures obtained in each χ_{SS} window were energy minimized with the same χ_{SS} constraints.

Average geometry characteristics of the molecules were calculated over 100 structures saved during each MD trajectory as follows. It has been shown[39] that for intramolecular fluctuations in a picosecond time scale NOE cross relaxation rate is proportional to $(r_{ij}^{-3})^2$, rather than to r_{ij}^{-6}. Therefore, for comparison with observed NOEs, interproton distances were averaged over MD structures as

$$r_{eff}(i,j) = \langle r_{ij}^{-3} \rangle^{-1/3} \quad (1)$$

Average $^3J_{NH\alpha}$ coupling constants were calculated according to the modified Karplus equation[27] with parameters taken from ref 27b.

Torsion angles were averaged over MD trajectories on a circular scale, in order to avoid incorrect estimates for angles distributed around the discontinuity point at ±180°. A value of a dihedral angle θ was represented by a slope of the unit vector $\mathbf{e}(\theta_i) = \{\cos\theta_i, \sin\theta_i\}$, and an average value of the angle θ was calculated through a slope of the average vector $\langle \mathbf{e}(\theta_i) \rangle$ as

$$\langle\theta\rangle = \arctan(\langle\sin\theta_i\rangle / \langle\cos\theta_i\rangle) \quad (2)$$

A standard deviation of the dihedral angle was calculated as a root-mean-square deviation of angle $\theta_i - \langle\theta\rangle$ between current vectors $\mathbf{e}(\theta_i)$ and the average vector $\langle \mathbf{e}(\theta_i) \rangle$, i.e. as

$$\langle\Delta\theta\rangle = [(1/n)\Sigma_i\{\arctan[\sin(\theta_i - \langle\theta\rangle)/\cos(\theta_i - \langle\theta\rangle)]\}^2]^{1/2} \quad (3)$$

where n is the total number of conformations. With this approach, torsion angles distributed around a *trans* conformation have average values of about ±180° with a small standard deviation, while the plain arithmetic averaging would result in averages about 0° with standard deviations of about 180°.

Results and Discussion

Nuclear Magnetic Resonance and Initial Model of Solution Structure. Corresponding ^{1}H and ^{13}C chemical shifts of the two OT-BC analogues (Tables 1 and 3) do not differ by more than 0.3 and 1.3 ppm, respectively, except for the chemical shifts of α protons and carbons of the Mpa^1 and dPen^1 residues. The sets of $^3J_{NH\alpha}$ coupling constants for the two peptides (Table 2) also are very similar. Temperature coefficients $\Delta\delta/\Delta T$ for amide protons range from 0.5 to 8.8 ppb/K for **1** and from 0.15 to 10.0 ppb/K for **2**, reflecting quite different solvent accessibilities of the amide protons of different residues.[40] In both analogues amide protons of the Ile^3 and Glu^4 residues seem to be screened from the solvent, and amide protons of residues 5 to 9 are accessible to the solvent. These data suggest a similar, well-defined conformation of analogues **1** and **2**, although small differences between coupling constants $^3J_{\alpha\beta}$ may reflect different conformational mobilities of the Tyr^2, Cys^6, and Lys^8 side chains in the two molecules (see Table 2).

NOESY spectra recorded at a mixing time $\tau_m = 100$ ms (see Figure 2) were shown to be free of spin diffusion. Unambiguously assigned NOE cross peaks were classified as strong (s), medium (m), and weak (w) correlations. The estimates of NOE intensities are given in Table 4. All sequential NH$_i$−C$^\alpha$H$_i$ and C$^\alpha$H$_i$−NH$_{i+1}$ NOEs were observed for **1**, while some of these NOEs were absent in the NOESY spectrum of **2** at $\tau_m = 100$ ms. Because similar rotational correlation times are expected for the two analogues, the difference in observed NOE patterns may be attributed to a more constrained conformational exchange in **2**. Comparing the relative intensities of the NOEs with the allowed ranges of distances between sequential NH and C$^\alpha$H protons in peptides,[41] we have concluded that weak NOEs observed at $\tau_m = 100$ ms correspond to the interproton distance cutoff of less than 4.0 Å, while strong and medium intensity NOEs correspond to interproton distances shorter than 2.5 and 3.0 Å, respectively. In order to justify the interproton distance evaluation, the motional behavior of **1** was probed by ^{13}C T_1 relaxation measurements.[33] The large similarity of C$^\alpha$ carbon T_1 relaxation times (225−235 ms) supports a conformationally rigid structure and suggests an isotropic overall tumbling of the molecule, vindicating the distance evaluation from NOE intensities.

^{1}H and ^{13}C NMR data revealed two distinct characteristics for the solution conformations of the OT-BC analogues in DMSO. First, the considerable differences between the ^{13}C chemical shifts of the C$^\beta$ and C$^\gamma$ carbons of Pro^7 (about 10 ppm for both OT-BC analogues; see Table 3) are typical for a *cis*-peptide bond for X-Pro.[42] The medium-intensity NOE cross-

(37) Polak, E.; Ribiere, G. *Rev. Fr. Informat. Recherche Operationelle* **1969**, *16*, 35; quoted from ref 35a.

(38) Ryckaert, J. P.; Cicotti, G.; Berendsen, H. J. C. *J. Comput. Phys.* **1977**, *23*, 327−341.

(39) Kessler, H.; Griesinger, C.; Lautz, J.; Müller, A.; van Gunsteren, W. F.; Berendsen, H. J. C. *J. Am. Chem. Soc.* **1988**, *110*, 3393−3396.

(40) (a) Kessler, H. *Angew. Chem., Int. Ed. Engl.* **1982**, *21*, 512−523. (b) Hruby, V. J. In *Chemistry and Biochemistry of Amino Acids, Peptides and Proteins*; Weinstein, B., Ed.; M. Dekker: New York, 1974; Vol. 3, pp 1−188.

(41) (a) Shenderovich, M. D.; Nikiforovich, G. V.; Chipens, G. I. *J. Magn. Reson.* **1984**, *59*, 1−12. (b) Shenderovich, M. D.; Nikiforovich, G. V.; Saulitis, J. B.; Chipens, G. I. *Biophys. Chem.* **1988**, *31*, 163−173.

(42) (a) Dorman, D. E.; Bovey, F. A. *J. Org. Chem.* **1973**, *38*, 2379−2383. (b) Grathwohl, C.; Wüthrich, K. *Bipolymers* **1981**, *20*, 2623−2633.

Table 4. NOE Correlations Observed for [Mpa[1]]OT-BC (**1**) and [dPen[1]]OT-BC (**2**), and Average Interproton Distances Calculated from Molecular Dynamics Trajectories at 300 K

	[Mpa[1]]OT-BC				[dPen[1]]OT-BC			
		av distances,[b] Å				av distances,[b] Å		
proton pairs	NOE intensity[a]	FMD-1L	DMD-1L	FMD-1R	NOE intensity[a]	FMD-2L	DMD-2L	FMD-2R
Y2 NH/Hα	m	2.9	2.9	2.9	w-m	2.9	2.9	2.9
Y2 NH/Hβ	m[d]	2.6	2.7	2.7	w-m(Hβ2)	2.7	2.9	2.4
Y2 NH/X1 Hα1	m[c]	2.5	2.6	2.5	w[c]	3.2	3.2	3.5
Y2 NH/X1 Hα2	m[c]	2.7	2.4	3.0	m[c]	2.3	2.3	2.3
Y2 NH/I3 NH	m-s[c]	2.2	2.2	2.2	m[c]	2.4	2.3	2.6
I3 NH/Hα	m	2.9	2.9	2.9		2.9	2.9	2.9
I3 NH/Y2 Hα	w	3.6	3.5	3.5		3.6	3.6	3.6
I3 NH/Y2 Hβ	m[d]	2.4	2.2	3.2	w(Hβ2)	2.3	2.3	2.4
I3 NH/E4 NH	s[c]	2.6	2.5	2.6	m-s[c]	2.4	2.4	2.5
E4 NH/Hα	w-m	2.9	2.9	2.9	w	2.9	2.9	2.9
E4 NH/Hβ	m[d]	2.7	2.6	3.1	w[d]	3.0	3.2	2.8
E4 NH/I3 Hα	w	3.6	3.6	3.6		3.5	3.3	3.6
N5 NH/Hα	w	2.9	2.9	2.9	w	2.9	2.9	2.9
N5 NH/Hβ	m[d]	2.4	2.5	2.5	m(Hβ2)	2.5	2.4	2.4
N5 NH/E4 Hα	s[c]	2.4	2.3	2.4	s[c]	2.5	2.4	2.4
N5 NH/E4 Hβ	w-m[d]	2.4	2.4	2.3	m[d]	2.3	2.4	2.4
C6 NH/Hα	w	2.9	2.9	2.9	w	2.9	2.9	2.9
C6 NH/Hβ2	w[d]	2.5	2.5	3.0	w	2.5	2.5	2.7
C6 NH/N5 Hα	s[c]	2.2	2.2	2.2	s[c]	2.2	2.2	2.2
C6 NH/N5 Hβ1	w[d]	*4.1*	*4.2*	*4.2*	w[d]	3.3	*4.3*	*4.2*
C6 Hα/Hβ1	m[c]	2.5	2.5	2.4	w[c]	2.5	2.5	2.5
C6 Hα/Hβ2	m[c]	3.0	3.0	2.4	w[c]	3.0	3.0	2.4
P7 Hα/Hβ1	m	2.3	2.3	2.3	m	2.3	2.3	2.3
P7 Hα/Hβ2	m	2.8	2.7	2.8	w	2.7	2.7	2.7
P7 Hα/C6 Hα	m[c]	2.3	2.4	2.3	m[c]	2.3	2.4	2.3
P7 Hα/C6 Hβ1	m[c]	2.8	2.2	*3.8*	w-m[c]	2.9	2.3	*3.9*
P7 Hα/C6 Hβ2	m[c]	*4.2*	*3.7*	2.7	w-m[c]	*4.3*	*3.8*	2.6
K8 NH/Hα	w	2.9	2.9	2.9		2.9	2.9	2.9
K8 NH/Hβ2	w[d]	2.5	3.3	2.5	w[d]	2.5	2.5	2.4
K8 NH/P7 Hα	s[c]	2.3	2.3	2.3	m-s[c]	2.3	2.3	2.3
K8 NH/P7 Hβ2	w-m	3.0	3.0	3.0	w	2.9	3.0	2.8
K8 NHζ/Hε1	m	2.6	2.7	2.7	w	2.5	2.6	2.7
K8 NHζ/Hε2	m	2.9	2.8	2.8	w	2.9	2.9	2.7
K8 NHζ/Hδ1,δ2	m[d]	2.8	2.8	2.9	w[d]	2.8	2.8	2.6
K8 NHζ/E4 Hγ	m[d]	2.4	2.3	2.3	m-s[d]	2.3	2.3	2.4
G9 NH/Hα	m[d]	2.6	2.6	2.6	w-m[d]	2.6	2.6	2.6
G9 NH/K8 Hα	m[c]	2.5	2.5	2.7	w-m[c]	2.4	2.5	3.2
av energy,[e] kJ/mol		416.5	439.7	426.1		451.7	462.4	456.4

[a] 2D NOESY experiments were carried out in DMSO-d_6 at 310 K with 100 ms mixing time. NOE cross-peak intensities were classified according to the number of contour levels as strong (s), medium-strong (m-s), medium (m), medium-weak (w-m), and weak (w). [b] Average interproton distances were calculated as $\langle r_{ij}^{-3}\rangle^{-1/3}$ over 100 structures saved during each MD trajectory. Distances inconsistent with the observed NOEs are italicized. Abbreviations for MD trajectories are as follows: FMD, free simulations; DMD, distance-restrained simulations; 1L, 1R, 2L, and 2R, analogues **1** and **2** with left-handed and right-handed chiralities of the disulfide bridge. [c] These NOEs were used to determine interproton distance constraints for distance-restrained MD simulations. [d] The shortest of two average distances is listed for geminal protons with overlapping resonances and in cases when the NOE observed for one of two geminal protons could not be assigned stereospecifically. [e] Average potential energies of MD trajectories scaled to 300 K.

peaks between the $C^{\alpha}H$ resonances of Cys[6] and Pro[7] observed for the two bicyclic analogues (see Figure 2b) also are characteristic of a *cis*-amide bond.[23] Taking into account that a single set of ^{1}H resonances was observed for each peptide, we conclude that conformers with a *cis*-amide bond Cys[6]−Pro[7] are populated up to 97% in DMSO. Second, the low temperature coefficients observed for amide protons of Ile[3] and Glu[4] ($\Delta\delta/\Delta T < 3.0 \times 10^{-3}$ ppm/K, Table 1), strong NH_i-NH_{i+1} NOE connectivities (Figure 2a), and weak $C^{\alpha}H_i-NH_{i+1}$ connectivities between protons of Tyr[2], Ile[3], and Glu[4] (or lack of them for **2**) are consistent with a reverse-turn conformation of residues 1 to 4. Moreover, the above NOE pattern is consistent with a type I or type III β-turn located at residues 2 and 3.[23]

Extensive conformational analysis of OT-BC[17] with the ECEPP/2[18] force field has been performed before the above NMR data became available. These calculations employed two "buildup" protocols which started with generation of low-energy conformations either for the 20-membered disulfide ring or for the 21-membered lactam ring (see Figure 1) and then proceeded to build the entire bicyclic structure. Several families of conformations satisfying the energy cutoff of 10 kcal/mol were selected for each OT-BC analogue. Comparison of these families with low-energy conformations of several potent monocyclic antagonists of OT allowed us to select three tentative models of biologically active conformations of OT-BC.[17] After the NMR studies of the bicyclic analogues were completed, representatives of all conformational families obtained with the ECEPP/2 force field were compared with NMR data (unpublished results), and the three models of [Mpa[1]]OT-BC suggested as putative biologically active conformations were tested more extensively[19] by MD simulations with the AMBER force field.[34] Although all conformations considered in the preliminary studies[17,19] had similar ranges of potential energies both in the ECEPP/2 and in the AMBER force fields, only one type of 3D structure possessed the conformational features discussed above, i.e. the type III β-turn at residues 2,3 and a *cis*-amide bond between Cys[6] and Pro[7], and was consistent with most of the NMR characteristics observed for analogue **1** in DMSO. This type of structure was selected in this study as the initial model of the solution conformation of OT-BC. Because NMR

Table 5. Comparison of Experimental Proton Coupling Constants $^3J_{NH\alpha}$ for [Mpa^1]OT-BC with Average $\langle ^3J_{NH\alpha}\rangle$ Values Obtained from Molecular Dynamics Simulations at 300 K

residue	exptl $^3J_{NH\alpha}$, Hz	expected φ angles[a]	av $\langle ^3J_{NH\alpha}\rangle$ and rms,[b] Hz			
			FMD-1L	FMD-1R	TMD-1L	TMD-1R
Tyr^2	8.9	−140, −100	7.1(2.1)	6.3(2.5)	8.6(1.0)	8.1(1.0)
Ile^3	8.9	−140, −100	5.1(2.2)	5.0(2.2)	8.3(1.0)	8.3(1.0)
Glu^4	7.1	−155, −85	6.9(2.3)	7.7(1.7)	7.3(1.2)	6.9(1.3)
Asn^5	6.9	−155, −85	7.0(2.1)	5.4(2.3)	6.7(1.0)	6.6(1.2)
Cys^6	8.2	−145, −95	8.5(1.8)	8.5(1.8)	8.7(0.9)	8.4(1.0)
Lys^8	8.2	−145, −95	5.9(1.9)	5.7(2.3)	7.6(1.0)	7.9(1.0)
av energy,[c] kJ/mol			416.1	426.1	420.1	433.1

[a] Expected values of φ angles are solutions of the Karplus−Bystrov equation[41] for experimental $^3J_{NH\alpha}$, rounded to the nearest 5°. Only negative solutions are shown, because only negative values of the φ angles were populated in MD simulations at 300 K. [b] Average $\langle ^3J_{NH\alpha}\rangle$ were calculated over 100 structures saved from each MD trajectory. RMS deviations are given in parentheses. Abbreviations for MD trajectories are as follows: FMD, free simulations; TMD, φ torsion-angle-restrained simulations; 1L, 1R, structures with a left-handed and a right-handed disulfide bridge, respectively. [c] Average potential energies of MD trajectories scaled to 300 K.

characteristics of the two OT-BC analogues are very similar (see Tables 1−3), we selected the lowest-energy conformations of **1** found in the preliminary MD simulations[19] as starting conformers for extensive MD study of the two bicyclic analogues of OT. Refinement of this model and evaluation of its dynamic properties, are described in the following paragraphs.

Free and Restrained Molecular Dynamics. Backbone Conformation. In order to evaluate the consistency of the selected model of solution structure with NMR data and to estimate the flexibility of backbone torsion angles in this model, free (nonrestrained) MD simulations at 300 K were carried out for OT-BC analogues **1** and **2**. The 100 ps free MD trajectories obtained for **1** and **2** will be referred to hereafter as FMD-1L, FMD-1R and FMD-2L, FMD-2R, respectively, where the abbreviations L and R refer to a left-handed ($\chi_{SS} = -90°$) or right-handed ($\chi_{SS} = 90°$) chirality of the disulfide bridge in starting conformations. Average interproton distances calculated over the MD trajectories (see eq 1) are shown in Table 4 in comparison with semiquantitative estimates of NOE cross-peak intensities. Similar sets of interproton distances were obtained for the two bicyclic peptides in MD simulations started both with left-handed and with right-handed conformers of the disulfide bridge. A satisfactory agreement between NOE intensities and average distances obtained in the free MD simulations is noteworthy. Most of the strong and medium NOEs correspond to average distances shorter than 3.0 Å, and weak NOEs correspond to distances shorter than 4.0 Å. The only discrepancy that concerns the NOEs and distances between the $C^\alpha H$ proton of Pro^7 and the $C^\beta H_2$ protons of Cys^6 will be discussed in the next paragraph.

Although free MD simulations confirmed consistency of the initial model of solution structure with experimental data, the robustness of this model was further tested upon introduction of distance constraints derived from the observed NOEs. Harmonic distance constraints with a force constant of 40 kJ/(mol·Å^2) and a flat-bottom well at 2.25 ± 0.25 Å were applied to the pairs of NH, $C^\alpha H$, and $C^\beta H$ protons corresponding to strong NOEs observed for [Mpa^1]OT-BC, and constraints with a force constant of 20 kJ/(mol·Å^2) and a flat-bottom well at 2.5 ± 0.5 Å were applied to pairs corresponding to medium NOEs. No restraints were applied for weak sequential $C^\alpha H_i - NH_i$ and $C^\alpha H_i - NH_{i+1}$ NOEs, as the estimated distance cutoff for a week NOE (4.0 Å) exceeds the natural upper limits of corresponding interproton distances (about 2.9 and 3.7 Å, respectively).[41] Although intensities of NOE cross peaks observed for **2** at $\tau_m = 100$ ms generally were lower than intensities of corresponding cross peaks observed for **1**, the same set of 13 distance constraints was applied to the two OT-BC molecules. Average interproton distances obtained from the distance-restrained trajectories DMD-1L and DMD-2L are given in Table 4. The distance-restrained MD did not change substantially the average interproton distance obtained by free MD, nor did they resolve the discrepancy that appeared for the $C^\beta H$ protons of Cys^6. An increase in the average potential energy of the distance-restrained MD trajectories (see Table 4) is due to additional bond stretching and van der Waals tension caused in an attempt to release the above distance violations. The energy difference between the restrained and free trajectories almost disappeared after removal of only two distance constraints between $C^\alpha H$ of Pro^7 and $C^\beta H_2$ of Cys^6.

Average values and root mean square (RMS) deviations of $^3J_{NH\alpha}$ coupling constants calculated from several MD trajectories for **1** are given in Table 5 in comparison with experimental $^3J_{NH\alpha}$ values. Free MD simulations (trajectories FMD-1L and FMD-1R in Table 5) resulted in high RMS deviations of $^3J_{NH\alpha}$ (about 2.0 Hz), and some of the average $^3J_{NH\alpha}$ obtained from these simulations deviate considerably from the experimental

Table 6. Average Torsion Angles of [Mpa^1]OT-BC and [dPen^1]OT-BC from Molecular Dynamics Simulations at 300 and 500 K

residue	torsion angles[a]	av angles (standard deviations), deg[b]			
		[Mpa^1]OT-BC		[dPen^1]OT-BC	
		FMD-1L	FMD-1R	FMD-2L	FMD-2R
Mpa^1	ψ'	−146.4(63)	−90.3(71)	100.4(40)	92.9(14)
dPen^1	$\chi^{1'}$	−179.3(11)	−155.1(48)	179.3(12)	−179.7(11)
	χ^2	−108.0(57)	81.2(61)	0.4(52)	−60.4(11)
Tyr^2	ϕ	−130.1(35)	−100.5(39)	−132.0(44)	−84.6(18)
	ψ	−52.6(14)	−31.8(22)	−57.7(15)	−56.7(16)
	χ^1	−179.0(12)	95.8(55)	−178.3(13)	−177.9(13)
	χ^2	68.2(23)	87.4(23)	49.3(102)	83.4(93)
Ile^3	ϕ	−73.3(15)	−72.6(18)	−83.7(21)	−78.6(16)
	ψ	−58.0(14)	−56.6(14)	−26.7(23)	−59.0(13)
	χ^1	−60.3(11)	−58.1(11)	60.0(13)	−61.3(12)
	χ^2	161.8(35)	169.0(29)	163.7(30)	158.1(38)
Glu^4	ϕ	−88.2(20)	−126.8(30)	−122.0(28)	−99.1(27)
	ψ	163.2(16)	173.2(23)	173.8(17)	167.1(16)
	χ^1	62.9(11)	60.1(10)	62.2(10)	62.6(11)
	χ^2	171.0(11)	173.3(11)	174.3(10)	176.2(11)
	χ^3	98.8(47)	88.0(36)	88.0(42)	80.3(46)
Asn^5	ϕ	−88.2(18)	−77.9(23)	−90.4(20)	−80.5(18)
	ψ	126.5(23)	120.0(25)	131.0(26)	117.6(23)
	χ^1	−177.1(12)	−178.0(12)	−109.7(59)	−176.8(11)
	χ^2	20.5(94)	−109.1(93)	−91.9(93)	51.0(80)
Cys^6	ϕ	−111.2(24)	−116.9(26)	−117.8(26)	−102.6(24)
	ψ	132.8(15)	134.4(16)	129.7(18)	141.6(17)
	χ^1	−70.7(10)	60.1(11)	−70.4(10)	71.9(12)
	χ^2	163.6(13)	−166.0(18)	171.9(11)	−165.8(10)
Pro^7	ω	2.6(11)	−2.2(11)	−0.9(11)	−5.3(9)
	ϕ	−75.5(9.5)	−71.9(10)	−71.8(10)	−75.5(9)
	ψ	153.4(13)	155.7(14)	155.4(12)	161.3(14)
Lys^8	ϕ	−79.0(15)	−77.5(16)	−80.2(14)	−77.9(19)
	ψ	77.8(88)	−33.2(92)	106.8(67)	−53.3(58)
	χ^1	−59.4(11)	−64.5(32)	−61.3(12)	−73.5(11)
	χ^2	−164.7(33)	−155.0(39)	−162.5(32)	122.2(47)
	χ^3	−168.6(12)	−168.6(29)	−169.4(14)	170.9(12)
	χ^4	−58.4(31)	−46.8(46)	−56.7(10)	63.6(14)
Gly^9	ϕ	155.1(73)	178.7(77)	156.9(77)	−137.4(78)
	ψ	108.3(93)	−19.5(96)	46.5(100)	52.7(92)
	χ_{SS}	−85.8(9)	89.9(11)	−97.0(10)	103.0(9)

[a] Nonconventional torsion angles ψ' ($C^\beta-C^\alpha-C'-N$) and $\chi^{1'}$ ($C^\gamma-C^\beta-C^\alpha-C'$) are given for the deamino residues in position 1; the torsion angle $C^\beta-S-S-C^\beta$ is denoted as χ_{SS}. [b] Average torsion angles and their standard deviations were calculated with eqs 2 and 3, respectively (see Experimental Section).

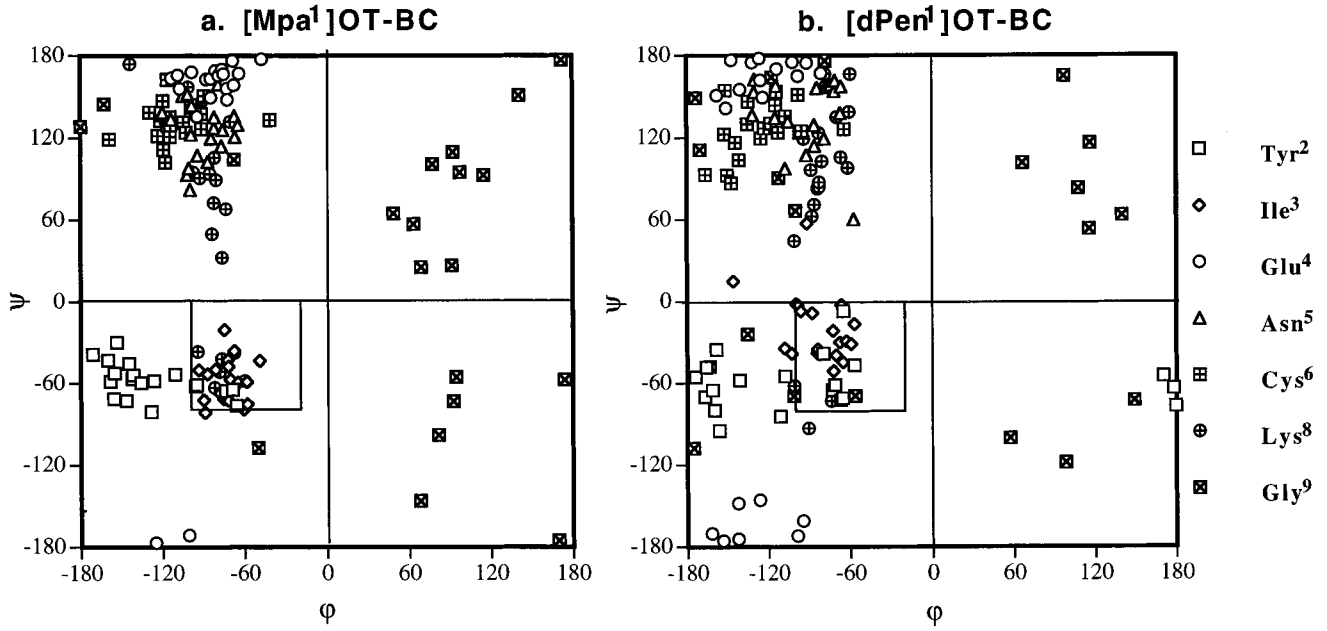

Figure 3. Distribution of the backbone torsion angles φ,ψ over the free MD trajectories for [Mpa[1]]OT-BC (a) and [dPen[1]]OT-BC (b) at 300 K. The φ,ψ angles are plotted for the conformations saved each 5 ps of MD trajectories which started from a left-handed conformer of the disulfide bridge. The φ,ψ values corresponding to the $i + 1$ and $i + 2$ residues in the type III β-turn[43] are shown by solid rectangles.

values. Although the φ values corresponding to experimental coupling constants were quite populated during free MD simulations (compare the expected values of φ angles in Table 5 with the average values and standard deviations of φ angles in Table 6), excessive fluctuations of φ angles and a random bias in their distributions seem to be responsible for systematic deviations of MD-averaged $^3J_{NH\alpha}$ toward the values lower than experimental ones. In order to test whether observed $^3J_{NH\alpha}$ values could be reproduced without a considerable change of the resulting structure or increase in its potential energy, the cosine constraints (see Experimental Section) with a force constant of 500 kJ/mol and a flat-bottom well at $\varphi_0 \pm 10°$ were applied to the φ angles of residues 2−6 and 8 in **1**. Two φ-angle-restrained MD trajectories (TMD-1L and TMD-1R) were collected starting from the same initial conformations that have been used for free MD simulations, and the centers of flat-bottom wells φ_0 were selected as the solutions of the modified Karplus equation[27] for the observed $^3J_{NH\alpha}$, closest to the corresponding φ values in the initial conformations. Average $^3J_{NH\alpha}$ obtained from these MD trajectories (Table 5) fit the experimental coupling constants within their standard deviations of about 1.0 Hz. It is noteworthy that the φ-angle-restrained simulations resulted in average structures close to those obtained by free MD, and that the average potential energies of the φ-angle-restrained trajectories were only a few kilojoules per mole higher than that obtained by free MD (see Table 5). Actually, the φ angle constraints allowed selection of subset of structures consistent with experimental $^3J_{NH\alpha}$ values from a total set of structures covered by the free MD simulations. These results also point out that free MD simulations may considerably overestimate the range of fluctuations allowed for the backbone torsion angles of a peptide in solution.

Average values and standard deviations of torsion angles calculated (see Experimental Section) from free MD trajectories at 300 K are given in Table 6. Distributions of (φ, ψ) torsion angles in conformations sampled from trajectories FMD-1L and FMD-2L with 5 ps time steps are plotted in Figure 3. It is noteworthy that four MD trajectories obtained for **1** and **2** starting from two different conformations resulted in very similar average backbone structures for residues 2 to 7. Although the free MD simulations may overestimate real intramolecular motions in solution (see above), standard deviations of torsion angles allow the moieties with lower and higher conformational mobility to be distinguished. Standard deviations of less than 30° obtained for φ, ψ angles of residues 3 to 7 indicate relatively low flexibility of the backbone segment between the C^α atoms of Tyr[2] and Lys[8]. In contrast, standard deviations of more than 60° for the ψ angle of Lys[8] and the φ,ψ angles of Gly[9] indicate almost free rotation of the exocyclic C-terminal moiety. Average values of the ψ angle of Tyr[2] and φ, ψ angles of Ile[3] fit the region defined as the type III β-turn ($\varphi = -60 \pm 40°$, $\psi = -30 \pm 40°$ [43]). Although the average φ angles of Tyr[2] deviate from the values expected for this type of β-turn, a considerable fraction of MD conformations of the Tyr[2] and Ile[3] residues falls into the classic type III β-turn region (see the squared regions of the φ, ψ plots in Figure 3), while the majority of conformations which deviate from the classical range only in the φ angle of Tyr[2] may be considered as distorted type III β-turns.

Thus, free MD simulations at 300 K revealed a stable backbone conformation, common for both OT-BC analogues, with the type III β-turn at the residues Tyr[2]-Ile[3]. The backbone of OT-BC forms another reverse turn at the Cys[6]-Pro[7] residues, which resembles a type VI β-turn structure[43] with a *cis*-peptide bond between residues 6 and 7. The reverse turn at residues 6−7, induced by the lactam cycle between residues 4 and 8, imposes a specific 3D folding of the C-terminal moiety of OT-BC, which cannot be easily attained in monocyclic analogues of OT. Space-filling stereoviews in Figure 4 illustrate the clearly amphiphilic character of the proposed solution structures of OT-BC analogues. Both molecules contain a polar surface (left sides of the molecules in Figure 4) that is formed by backbone CO and NH groups, the polar side chain of Asn[5], and the hydroxyl group of Tyr[2]. The opposite, predominantly hydrophobic side of the molecules (right side in Figure 4) is formed by the side chains of residues 1−3 and 6−8. The main difference between analogues **1** and **2** is that a small polar grove separating two hydrophobic regions in **1** (Figure 4, top) is filled in **2** by two bulky β-methyl groups of dPen[1] (Figure 4, bottom), so that the

(43) Lewis, P. N.; Momany, F. A.; Scheraga, H. A. *Biochim. Biophys. Acta* **1973**, *303*, 211−229.

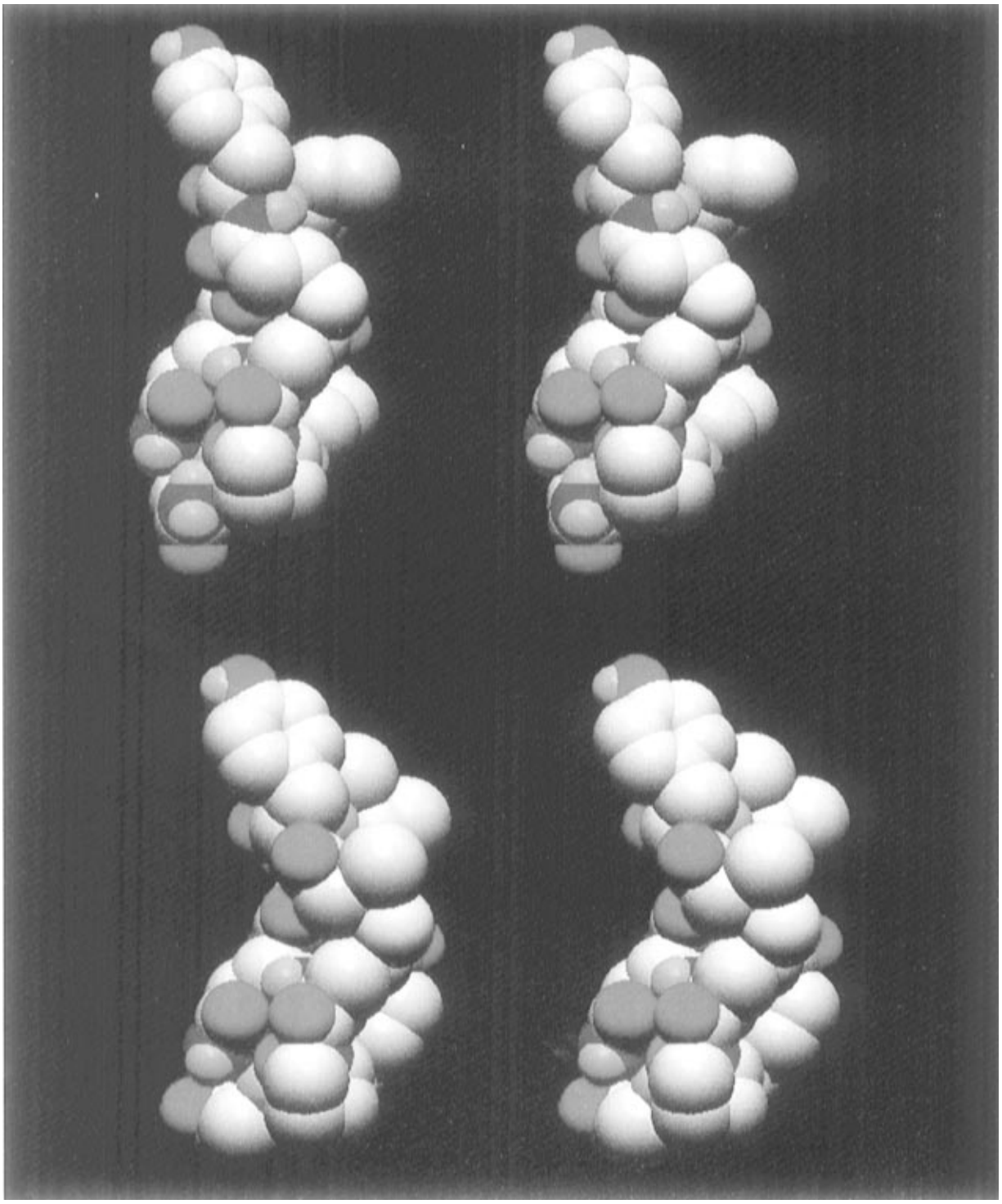

Figure 4. Space-filling stereoviews of the lowest-energy conformations of [Mpa[1]]OT-BC (top) and [dPen[1]]OT-BC (bottom). The hydrophobic (right side) and polar (left side) surfaces of the molecules can be distinguished. Atom color codes: C, white; O, red; N, blue; S, yellow; O*H*, light red; N*H*, light blue.

latter analogue has a continuous hydrophobic surface. The amphiphilic structure with the distinct polar and hydrophobic surfaces may play an important role upon binding of the bicyclic antagonists to the oxytocin receptor.

Conformational Transitions of the Disulfide Bridge. The main contradiction between NMR data and results of MD simulations at 300 K concerns NOEs between the $C^{\beta}H_2$ protons of Cys[6] and the $C^{\alpha}H$ proton of Pro[7]. Two medium-intensity NOEs observed for each OT-BC analogue suggest a close proximity between *both* $C^{\beta}H$ protons of Cys[6] and the $C^{\alpha}H$ of Pro[7]. In contrast, MD simulations predicted quite different average distances for the two proton pairs (less than 3.0 Å and about 4.0 Å; Table 4), even when distance constraints with the upper limit of 3.0 Å were explicitly applied to these proton pairs. Furthermore, the $^3J_{\alpha\beta}$ coupling constants of 8.2 Hz and less than 1.0 Hz (see Table 2) suggested almost equal population of two χ^1 rotamers of Cys[6] in **1**, which were tentatively assigned as the *gauche (−)* and *gauche (+)* rotamers. The $^3J_{\alpha\beta}$ values for Cys[6] in **2** (Table 2) also are consistent with an equilibrium of the two χ^1 rotamers, although in this case a higher population of the *gauche (−)* rotamer is expected. In order to explain these experimental data, we have suggested[19] an equilibrium between disulfide bridge conformers of a left-handed helicity ($\chi_{SS} = -90°$) with a *gauche (−)* χ^1 rotamer of Cys[6] and conformers

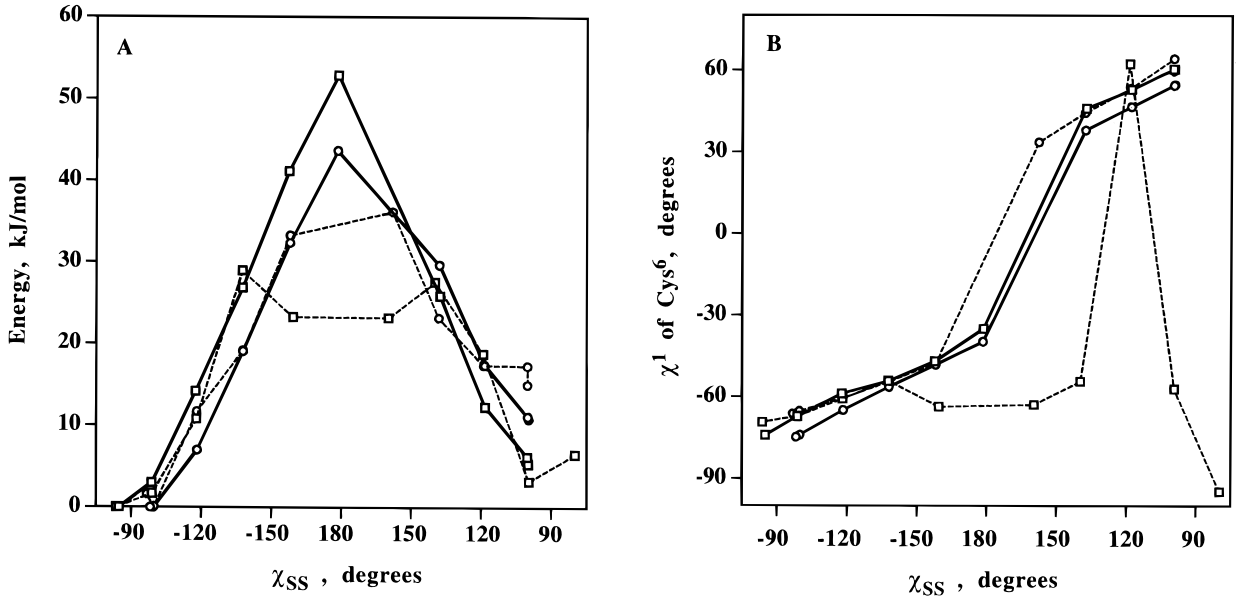

Figure 5. Potential energy profiles (panel A) and evolution plots of the χ^1 torsion angle of Cys^6 vs the χ_{SS} angle (panel B) for the induced disulfide bridge transitions in [Mpa^1]OT-BC (squares) and [dPen^1]OT-BC (circles). Solid lines correspond to transitions induced by the χ_{SS}-restrained energy minimization, and dashed lines correspond to transitions obtained by continuous MD simulations with shifting χ_{SS} constrains (for details see the Experimental Section).

of a right-handed helicity ($\chi_{SS} = 90°$) with a *gauche (+)* χ^1 rotamer of Cys^6. In these two conformations *two different* C$^\beta$H protons of Cys^6 have short average distances to the C$^\alpha$H proton of Pro^7 (Table 4), and therefore, two medium-intensity NOEs may be observed upon a fast dynamic exchange between the disulfide bridge conformers. However, MD simulations at 300 K did not reveal the expected conformational transitions. Torsional barriers at the *trans* ($\chi_{SS} = 180°$) and *cis* ($\chi_{SS} = 0°$) conformations of the S−S bond in dimethyl disulfide have been estimated at 26 and 48 kJ/mol, respectively.[44] Apparently, the energy barriers of rotation around the disulfide bond are considerably higher than the energy fluctuations of a few k_BT that can be sampled during short MD runs at room temperature.

In order to confirm the possibility of transitions between left-handed and right-handed conformers of the disulfide bridge, two forced-transition protocols (see Experimental Section) have been applied to the proposed solution conformations of OT-BC. In these calculations we have assumed that the torsion angle χ_{SS} roughly represents a coordinate of disulfide bridge transitions. The χ_{SS} angle was driven by a strong penalty potential between two equilibrium values at ±90° over the energy barriers at $\chi_{SS} = 180°$. A transition trajectory was represented by a series of "snapshot" conformations, energy-minimized in each χ_{SS} window, and a barrier of transition was estimated as the difference between the maximum and minimum of potential energy along the trajectory.

Potential energy profiles of the induced disulfide bridge transitions are shown in Figure 5A; evolutions of the χ^1 angle of Cys^6 that follow the induced shift of the χ_{SS} angle are plotted in Figure 5B. Very similar transitions between left-handed conformers with a *gauche (−)* rotamer of Cys^6 and right-handed conformers with a *gauche (+)* rotamer of Cys^6 were obtained for the two analogues by energy minimization with the gradually shifting χ_{SS} constraints (solid lines in Figure 5). Potential energy barriers for these transitions amount at about 50 and 45 kJ/mol for **1** and **2**, respectively, and differences between two energy minima are about 5 and 10 kJ/mol, respectively, in favor of the left-handed conformer. Transitions over such energy barriers may be fast enough to observe a single set of NOE cross peaks with time-averaged intensities, and the energy differences between the equilibrium conformers are consistent with the assignment and populations of the two χ^1 rotamers of Cys^6 in **1** and **2** given in Table 2. However, the second protocol which employed continuous MD simulations with gradually shifting χ_{SS} constraints (dashed lines in Figure 5) has revealed quite different conformational mobility of the disulfide bridges in two OT-BC analogues. For [dPen^1]-OT-BC both protocols gave similar transition trajectories with correlated changes of the χ_{SS} angle and the χ^1 angle of Cys^6 (see Figure 5B), although the MD relaxation resulted in a decrease of the barrier height to about 35 kJ/mol. In contrast, because of a higher conformational mobility of the Mpa^1 residue, transitions between left- and right-handed disulfide bridge conformers of **1** may take place without a simultaneous transition between χ^1 rotamers of Cys^6. In the trajectory shown in Figure 5B, both equilibrium conformers have a *gauche (−)* χ^1 rotamer of Cys^6, although a *gauche (+)* rotamer has appeared in an intermediate step of this transition. Such a "non-correlated" transition has a relatively low energy barrier of about 30 kJ/mol, which is comparable to the 26-kJ/mol barrier found by quantum chemistry calculations for dimethyl disulfide.[44] Moreover, because the two χ^1 rotamers have almost equal energies and may be separated by a low-energy barrier, independent transitions along the χ^1 coordinate may follow the major transition in the χ_{SS} dimension. Such multistep transitions in the disulfide bridge moiety of **1** were found by MD simulations at 500 K.

Molecular Dynamics at 500 K. Conformational Mobility of Side Chains. The values of $^3J_{\alpha\beta}$ coupling constants measured in DMSO (Table 2) suggest an equilibrium of two or three staggered χ^1 rotamers for almost all side chains in the two analogues. However, transitions between side chain conformers were rarely observed during MD simulations at 300 K. In order to investigate more extensively the conformational mobility of individual side chains in OT-BC, we have performed additional MD simulations at 500 K. As was shown recently for cyclosporine A,[45] MD simulations at a reasonably high tem-

(44) Jiao, D.; Barfield, M.; Combariza, J. E.; Hruby, V. J. *J. Am. Chem. Soc.* **1992**, *114*, 3639−3643.

(45) O'Donohue, M. F.; Burgess, A. W.; Walkinshaw, M. D.; Treutlein, H. R. *Protein Sci.* **1995**, *4*, 2191−2202.

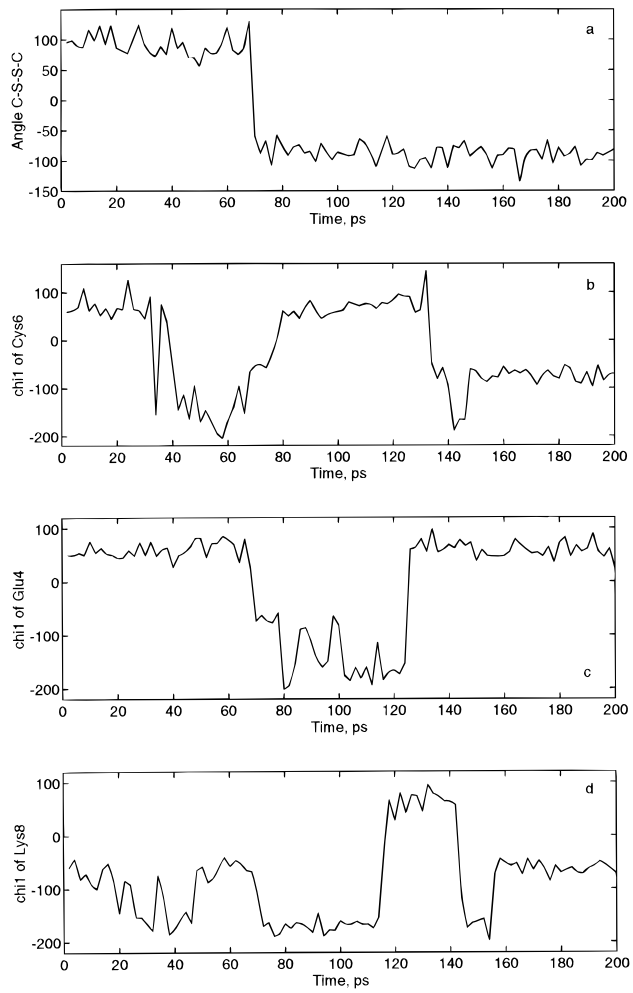

Figure 6. Evolution of selected torsion angles of [Mpa[1]]OT-BC during MD simulations at 500 K: a, dihedral angle $C^{\beta}-S-S-C^{\beta}$ (χ_{SS}); b, χ^1 of Cys[6]; c, χ^1 of Glu[4]; d, χ^1 of Lys[8].

perature are able to reproduce correctly conformational transitions in cyclic peptides of this size. The temperature of these simulations was chosen as a compromise that "speeded-up" transitions over relatively small energy barriers, but did not "heat-up" the molecules to unreasonable potential energies. Average structures obtained from most MD trajectories at 500 K were fairly close to those obtained at 300 K, and the backbone structure with a β-turn at residues 2,3 still was the most populated one for both OT-BC analogues.

Perhaps the most interesting result of MD simulations at 500 K is the spontaneous transitions in the disulfide bridge moiety of [Mpa[1]]OT-BC observed in trajectories which started from a right-handed conformer with the *gauche (+)* χ^1 rotamer of Cys[6]. Time evolutions of the χ_{SS} and χ^1 torsion angles during one of these trajectories are shown in Figure 6, plots a and b. A very fast transition between two equilibrium χ_{SS} conformers took place at about 70 ps in the trajectory, and was completed in a few picoseconds (Figure 6a). It was initiated and followed by slower transitions or fluctuations which involved almost all χ angles of the disulfide bridge and backbone torsion angles of residues 1 to 3. First, between 30 and 50 ps the χ^1 angle of Cys[6] moved from a *gauche (+)* to a *trans* rotamer (Figure 6b). This resulted in a high-energy structure that rapidly relaxed by a simultaneous transition of the χ_{SS} angle, χ angles of Mpa[1] and Cys[6], and the backbone angles of Tyr[2] and Ile[3]. For the next 60 ps the molecule was in a transition state with a left-handed disulfide bridge, *gauche (+)* conformation of the Cys[6] side chain, and a disrupted or considerably deformed β-turn at residues 2,3. The type III β-turn was restored after the next rotamer transition in the Cys[6] side chain, which took place at about 140 ps (see Figure 6b), and for the last 50 ps of this trajectory the molecule had a quite stable structure with a left-handed disulfide bridge and a *gauche (−)* rotamer of Cys[6]. Thus, the transition between two stable conformers of the disulfide bridge in **1** had a stepwise character with a rapid switch of the disulfide bridge chirality, several consecutive rotamer transitions in the Cys[6] side chain, and a temporary disruption of the β-turn at residues 2,3 in a transition structure. As was shown in the previous paragraph, such a stepwise transition has a relatively low energy barrier that allows a fast conformational exchange at the NMR time scale. In contrast, for analogue **2** with the conformationally constrained dPen[1] side chain, the disulfide bridge transition has a higher energy barrier and should involve several torsion angles simultaneously. Such correlated transitions have not been observed in free MD simulations for **2** even at 500 K.

MD simulations at 500 K have revealed also conformational transitions in the lactam bridge moieties of both OT-BC analogues formed by the side chains of Glu[4] and Lys[8]. Plots c and d in Figure 6 show time evolution of the χ^1 torsion angles of Glu[4] and Lys[8] in **1** along the MD trajectory discussed above. A major rearrangement of the lactam bridge moiety started simultaneously with the fast change of the disulfide bridge chirality (cf. plots a, c, and d in Figure 6), and in the middle part of the trajectory the lactam bridge assumed several conformations with different combinations of χ^1 rotamers of the two side chains. After the disulfide bridge transitions have been completed, the lactam bridge moiety also assumed an equilibrium conformation with a *gauche (+)* rotamer of Glu[4] and a *gauche (−)* rotamer of Lys[8]. Transitions in the lactam bridge moieties of **1** and **2** observed in the high-temperature MD simulations are qualitatively consistent with experimental $^3J_{\alpha\beta}$ coupling constants for the Glu[4] and Lys[8] side chains in DMSO (see Table 2). In addition, rotamer transition in the side chains of Tyr[2] and Asn[5] was quite often observed during MD simulations at 500 K, which apparently reflects small energy differences and relatively low barriers between χ^1 rotamers of these side chains.

The induced conformational transitions in the disulfide bridge moiety and the spontaneous transitions observed during high-temperature MD allow us to suggest a dynamic model of the three-dimensional structure of OT-BC analogues. This model assumes the stable backbone structure described in previous paragraphs for conformationally flexible disulfide bridge and lactam bridge moieties. The dynamic model is illustrated in Figure 7 by superposition of three low-energy conformations of [Mpa[1]]OT-BC which combine alternative conformers of the disulfide and lactam bridges found in this sudy. Torsional angles of the lowest-energy conformations of **1** and **2** with the left-handed and right-handed disulfide bridge are given in the Supporting Information.

Structure−Activity Relationships of Oxytocin Antagonists. The solution structure of OT-BC analogues suggested in this study was quite stable during various MD simulations at 300 and 500 K. CD spectra of OT-BC are consistent with a similar backbone structure of **1** and **2** in trifluoroethanol and in aqueous solution.[20] These data allow us to assume that the 3D structure of OT-BC is relatively stable upon environmental changes and to consider the suggested solution structure as a putative model for the uterine receptor-binding conformation of the bicyclic antagonists. The most characteristic features of this model, namely the β-turn located at residues 2,3 and the *cis*-amide bond between Cys[6] and Pro[7], seem quite unexpected from the

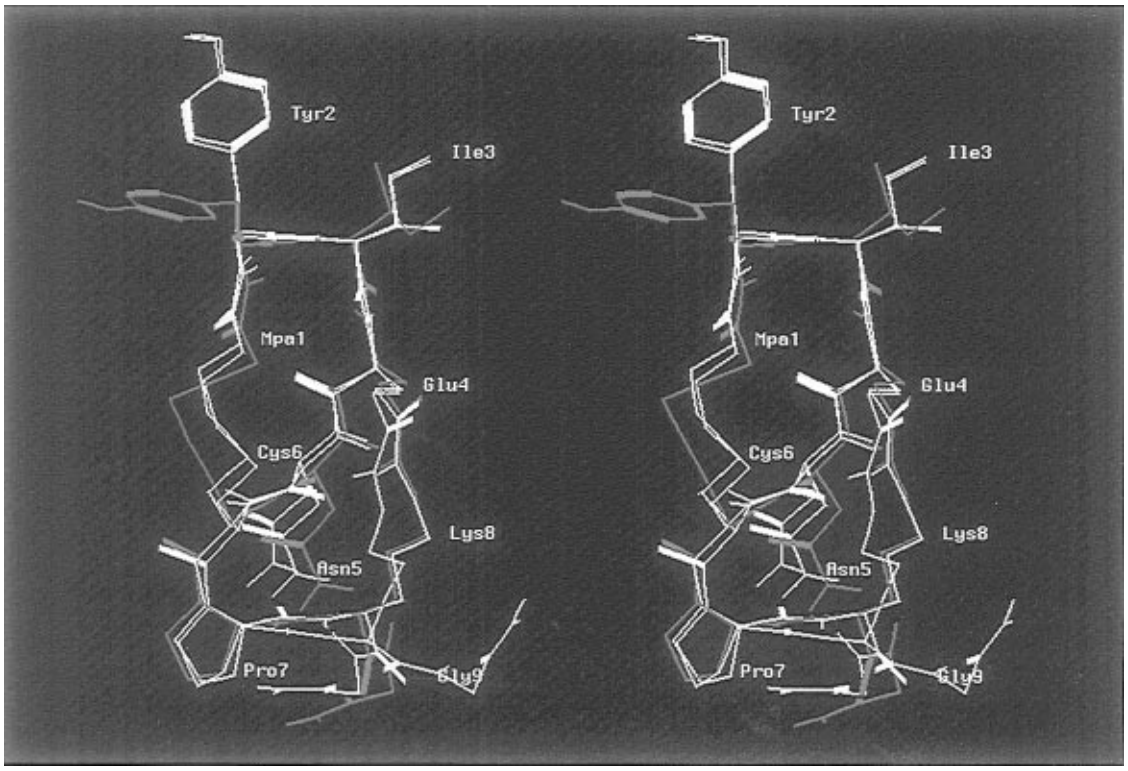

Figure 7. A dynamic model of the solution structure of [Mpa[1]]OT-BC. The model is represented by superposed stereoviews of the low-energy conformations with left-handed (white) and right-handed (red) conformers of the disulfide bridge, and with an alternative conformer of the lactam bridge (yellow).

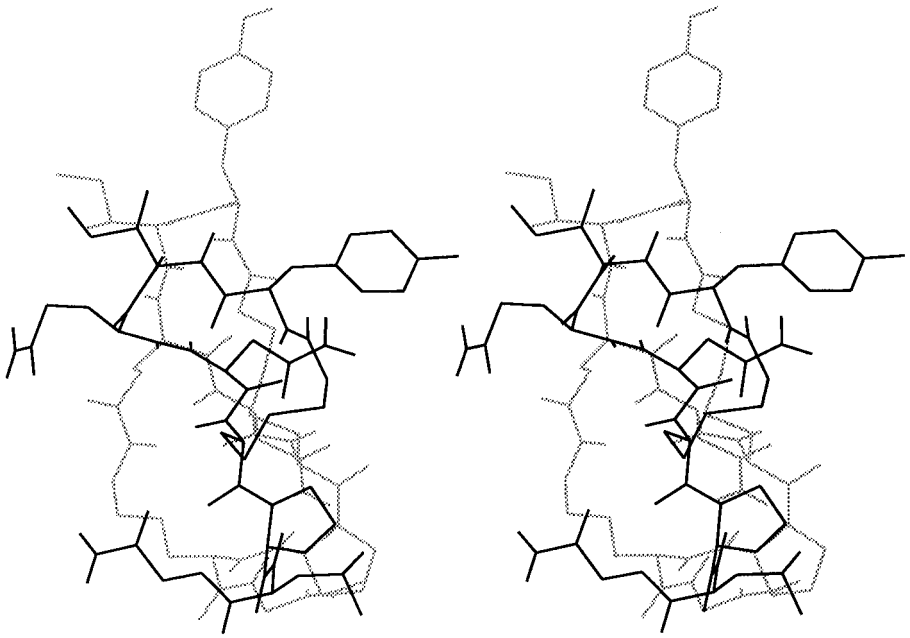

Figure 8. Superposition of the crystal conformation of deamino-oxytocin[9] (solid lines) and the solution conformation of [Mpa[1]]OT-BC (shadow lines). The superposition was performed by a best-fit matching of C^{α} and C^{β} atoms of residues 2 to 8 in the conformers with a left-handed disulfide bridge.

traditional point of view on conformation−activity relationships of OT analogues. First, in the 3D model proposed by Urry and Walter,[6] a structure with a β-turn at residues 3,4 was suggested as the biologically active conformation of OT. This opinion has been supported by the crystal structure of deamino-oxytocin ([Mpa[1]]OT),[9] which possesses a type II β-turn at residues 3,4 and by further structure−activity studies.[2,3] Superposed stereoviews of the crystal conformation of [Mpa[1]]OT and the lowest-energy conformation of [Mpa[1]]OT-BC found in this study are shown in Figure 8. This superposition, performed by a best-fit matching of C^{α} and C^{β} atoms of residues 2 to 8 (RMS = 3.9 Å), illustrates the difference in 3D structures of the potent agonist and antagonist of OT. Second, a *trans* conformation of the amide bond Cys[6]−Pro[7] was observed both in the crystal structure[9] and in solution structures of OT analogues.[46] It has been suggested already that agonists and

(46) (a) Larive, C. K.; Guerra, L.; Rabenstein, D. L. *J. Am. Chem. Soc.* **1992**, *114*, 7331−7337. (b) Hruby, V. J.; Brewster, A. I.; Glasel, J. A. *Proc. Natl. Acad. Sci. U.S.A.* **1971**, *68*, 450−453. (c) Brewster, A. I.; Hruby, V. J. *Proc. Natl. Acad. Sci. U.S.A.* **1973**, *70*, 3806−3809.

Table 7. Structural Diversity of Oxytocin Antagonists

compd[a]	pA_2	ref
1. [Mpa^1,*cyclo*(Glu4,Lys8)]OT	8.2	16
2. [dPen^1,*cyclo*(Glu4,Lys8)]OT	8.7	17
3. [D-Phe^2]OT	7.3	48a
4. [Cpp^1]OT	7.6	48b
5. [dPen^1,Phe2]OT	7.8	48c
6. [Cpp^1,D-Phe^2,Phe^3,Arg^8]OT	8.6	49
7. [Cpp^1,D-Trp^2,Arg^8]OT	7.8	50
8. [Cpp^1,D-Trp^2,D-Cys^6,Arg^8]OT	8.3	50
9. [Cpp^1,D-Trp^2,D-Pro^7,Arg^8]OT	7.9	50
10. *cyclo*(Pro-D-Phe-Ile-D-Pip-Pip-D-NMePhe)	8.6	51
11. L-366,509	7.3	52

[a] Abbreviations for non-usual amino acids: Mpa, β-mercaptopropionic acid (deaminocysteine); dPen, β,β-dimethyl-β-mercaptopropionic acid (deaminopenicillamine); Cpp, β,β-cyclopentamethylene-β-mercaptopropionic acid; Pip, piperidine-2-carboxylic acid (pipecolic acid).

antagonists interact in a different manner with the oxytocin receptor.[47] Results of the present study contribute additional evidence in support of this hypothesis.

Structures and activities of the bicyclic analogues **1** and **2** and a few of the most potent antagonists of OT are compared in Table 7. Selection of compounds in Table 7 was made to illustrate the high structural diversity of potent inhibitors of the uterotonic activity of OT (pA_2 > 7.0). In early studies OT antagonists have been produced by substitution of Tyr^2 with aromatic D-amino acids (analogue **3**) and/or by introduction of bulky β-substituents into position 1 (analogues **4** and **5**).[48] A D-amino acid substitution may change a preferred orientation of the aromatic side chain in position 2 and enhance a β-turn conformation at residues 1 to 4. Bulky β-substituents increase hydrophobicity of residue 1 and constrain conformational mobility of the disulfide bridge moiety.[12] All these effects may shift conformational equilibrium of OT analogues toward an antagonist-binding conformation. A combination of the above modifications and the presence of the bulkier Phe residue in position 3 led to the vasopressin analogue **6,**[49] one of the most potent uterotonic antagonists known before the discovery of the bicyclic analogues of OT.

It should be noted that the first bicyclic antagonist, [Mpa^1]-OT-BC,[16] did not contain the "traditional" modifications in the N-terminal part. Residues 1, 2, and 3 in this analogue are exactly the same as in the superpotent agonist [Mpa^1]OT. Furthermore, the monocyclic precursor of OT-BC, [Mpa^1,Glu^4,-Lys^8]OT, was a weak uterotonic agonist,[16] and neither this analogue nor the related analogue [Mpa^1,Lys(CHO)^8]OT[17] with electroneutral side chains in positions 4 and 8 showed any antagonistic activity. Therefore, the potent antagonism of **1** was caused solely by strong conformational constraints imposed by additional cyclization between the side chains in positions 4 and 8. Present NMR and MD study has revealed the exact nature of these conformational constraints. The "traditional" substitution of Mpa^1 with dPen^1 in the bicyclic sequence resulted in a 3-fold increase of the antagonistic potency. As was shown in this study, two bicyclic analogues have similar 3D structure, although additional β-methyl groups expand the continuous hydrophobic region in the N-terminal part of OT-BC (see Figure 4) and reduce conformational mobility of the disulfide bridge moiety. Both these effects may be responsible for the enhanced affinity of [dPen^1]OT-BC to an antagonist-binding site of the OT receptor.

The *cis* conformation of the Cys^6−Pro^7 amide bond is, perhaps, the most challenging feature of the bicyclic antagonists. It induces a reverse turn at residues 6,7 and a specific "backward" folding of the C-terminal tripeptide, which cannot be easily attained in a majority of the monocyclic analogues. In this context, results of D-amino acid substitutions in the antagonist [Cpp^1,D-Trp^2,Arg^8]OT (analogue **7** in Table 7), reported recently by Flouret et al.,[50] are noteworthy. The D-Pro^7 substitution (**8**) retained full antagonistic potency of the parent analogue, whereas D-Cys^6 substitution (**9**) resulted in an increased antagonistic potency. The D-amino acids in positions 6 and 7 should change considerably the preferred orientation of the C-terminal moiety. In particular, the D-Cys^6 modification may result in reverse folding similar to that induced via *cis* conformation of the amide bond Cys^6−Pro^7 in OT-BC. This specifically constrained conformation of the C-terminal moiety may be the common reason for enhanced receptor interactions of the monocyclic antagonist **9** and of the bicyclic antagonists **1** and **2**. Further modifications are necessary to find out whether the C-terminal moiety contributes directly to the receptor binding of the OT antagonists.

Compounds **10** and **11** in Table 7 represent two series of uterotonic antagonists that are not related directly to the amino acid sequences of neurohypophyseal hormones. In the cyclic hexapeptide antagonists[51] only the tripeptide Pro-D-Phe-Ile is homologous to N-terminal sequences of the OT antagonists that contain a hydrophobic residue in position 1 and a D-amino acid in position 2. This structural homology suggests that N-terminal tripeptides of all OT antagonists may interact with the same hydrophobic site of the receptor. Although the second tripeptide of the cyclic hexapeptides does not resemble any part of the OT sequence, it should be involved in receptor binding to achieve a high antagonistic potency. In particular, the highly hydrophobic D-NMePhe residue in the most potent antagonist of this series (**10**) may fit a possible binding site for the Pro^7-Lys^8 dipeptide of the bicyclic analogues.

The non-peptide antagonist L-366,509[52] (**11**) contains spiroindene and camphor moieties which are structurally related to the tyrosine and isoleucine residues of OT, respectively. This compound apparently represents the minimum structural requirements for OT antagonists. A good overlap between a non-peptide antagonist related to **11** and a cyclic hexapeptide related to **10** was recently reported.[53] Therefore, fitting of L-366,509 to the Tyr^2-Ile^3 dipeptide of OT-BC in its β-turn conformation was considered as an important test of the proposed 3D model.[54]

(47) (a) Hruby, V. J. *Trends Pharmacol. Sci.* **1987**, *8*, 336−338. (b) Meraldi, J.-P.; Hruby, V. J.; Brewster, A. I. R. *Proc. Natl. Acad. Sci. U.S.A.* **1977**, *74*, 1373−1377.

(48) (a) Lebl, M.; Hill, P.; Kazmierski, W.; Kárászová, L.; Slaninová, J.; Fric, I.; Hruby, V. J. *Int. J. Pept. Protein Res.* **1990**, *36*, 321−330. (b) Lowbridge, J.; Manning, M.; Seto, J.; Haldar, J.; Sawyer, W. H. *J. Med. Chem.* **1979**, *22*, 565−569. (c) Kruszynski, M.; Lammek, B.; Manning, M.; Seto, J.; Haldar, J.; Sawyer, W. H. *J. Med. Chem.* **1980**, *23*, 364−368.

(49) Manning, M.; Olma, A.; Klis, W. A.; Seto, J.; Sawyer, W. H. *J. Med. Chem.* **1983**, *26*, 1607−1611.

(50) Flouret, G.; Majewski, T.; Brieher, W. *J. Med. Chem.* **1993**, *36*, 747−749.

(51) (a) Williams, P. D.; Bock, M. G.; Tung, R. D.; Garsky, V. M.; Perlow, D. S.; Erb, J. M.; Lundell, G. F.; Gould, N. P.; Whitter, W. L.; Hoffman, J. B.; Kaufman, M. J.; Clineschmidt, B. V.; Pettibone, D. J.; Freidinger, R. M.; Veber, D. F. *J. Med. Chem.* **1992**, *35*, 3905−3918. (b) Pettibone, D. J.; Clineschmidt, B. V.; Bock, M. G.; Evans, B. E.; Freidinger, R. M.; Veber, D. F.; Williams, P. D. *Regul. Pept.* **1993**, *45*, 289−293.

(52) (a) Evans, B. E.; Leighton, J. L.; Rittle, K. E.; Gilbert, K. F.; Lundell, G. F.; Gould, N. P.; DiPardo, R. M.; Veber, D. F.; Pettibone, D. J.; Clineschmidt, B. V.; Anderson, P. S.; Freidinger, R. M. *J. Med. Chem.* **1992**, *35*, 3919−3927. (b) Pettibone, D. J.; Clineschmidt, B. V.; Kishel, M. T.; Lis, E. V.; Reiss, D. R.; Woyden, C. J.; Evans, B. E.; Freidinger, R. M.; Veber, D. F.; Cook, M. J.; Haluska, G. J.; Novy, M. J.; Lowensohn, R. I. *J. Pharmacol. Exp. Ther.* **1993**, *264*, 308−314.

(53) Williams, P. D.; Anderson, P. S.; Ball, R. G.; Bock, M. G.; Carroll, L.; Chiu, S.-H. L.; Clineschmidt, B. V.; Culberson, J. C.; Erb, J. M.; Evans, B. E.; Fitzpatrick, S. L.; Freidinger, R. M.; Kaufman, M. J.; Lundell, G. F.; Murphy, J. S.; Pawluczyk, J. M.; Perlow, D. S.; Pettibone, D. J.; Pitzenberg, S. M.; Thompson, K. L.; Veber, D. F. *J. Med. Chem.* **1994**, *37*, 565−571.

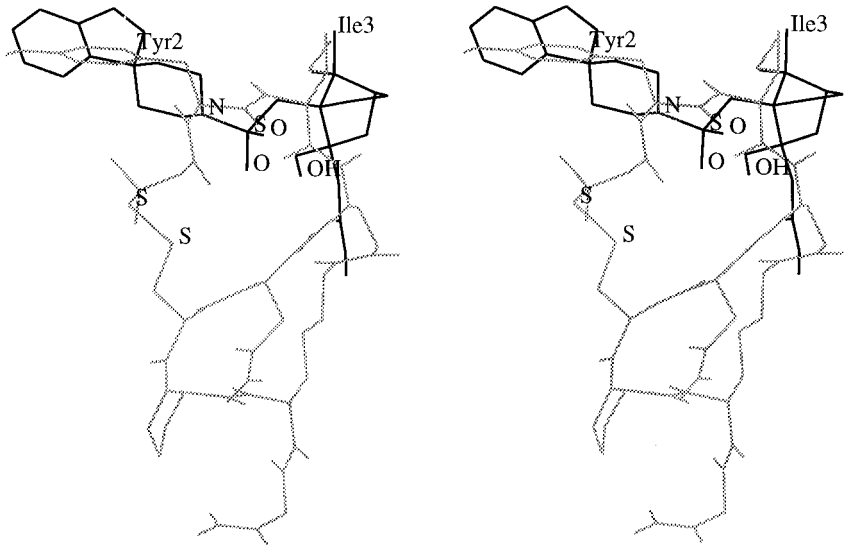

Figure 9. Superposition of the non-peptide oxytocin antagonist L-366,509[52] (solid lines) with the Tyr[2]-Ile[3] dipeptide of [dPen[1]]OT-BC (shadow lines).

Figure 9 shows an overlap between representative low-energy conformations of [dPen[1]]OT-BC and L-366,509. This example illustrates the possibility of a good fitting between the non-peptide antagonist and the Tyr[2]-Ile[3] moiety of OT-BC with a tight overlap of the aromatic rings and exact matching of the camphor moiety and the Ile[3] side chain. Furthermore, upon this fitting one of the sulfonamide oxygens of L-366,509 overlaps with the carbonyl oxygen of Tyr[2], and the hydroxyl group attached to the camphor moiety is located close to the carbonyl oxygen of Ile[3]. Therefore, the non-peptide antagonist and the Tyr[2]-Ile[3] moiety of OT-BC may fit to the same antagonist-binding site of the uterine OT receptor.

Conclusions

The combined approach including ^{1}H and ^{13}C NMR spectroscopy, computer modeling, and molecular dynamics simulations allowed us to determine the three-dimensional structure of the potent bicyclic antagonists of oxytocin in DMSO solution. The proposed 3D model is characterized by the type III β-turn located at the Tyr[2]-Ile[3] residues and by the *cis*-amide bond between Cys[6] and Pro[7], which induces a reverse turn in the C-terminal moieties of the bicyclic peptides. The disulfide bridge and the lactam bridge moieties of two analogues are relatively flexible with respect to the constrained backbone conformation. The solution structure of OT-BC differs considerably from the crystal structure of deaminooxytocin[9] and from solution structures proposed for OT analogues.[6] This fact confirms the hypothesis[47] that agonists and competitive antagonists of OT may interact somewhat differently with the uterine receptor of OT.

The high stability of the backbone conformation of OT-BC during various MD simulations allowed us to consider the proposed solution structure as a tentative model for the biologically active conformation of the bicyclic analogues. This model is generally consistent with structure−activity relationships of OT antagonists. In particular, a β-turn-like conformation in the N-terminal part seems to be the common feature of all potent OT antagonists that may be stabilized by subsitution of Tyr[2] with a D-amino acid. A good overlap of a non-peptide antagonist of OT with the Tyr[2]-Ile[3] dipeptide of OT-BC suggests that this moiety is responsible for a specific binding of antagonists to the OT receptor. The location of the Asn[5] side chain at the top of a polar surface of OT-BC suggests a direct involvement of this side chain in antagonist−receptor interactions. Although this study has revealed the constrained, specifically folded conformation in the C-terminal part of OT-BC, the role of this moiety in the antagonist−receptor binding is still unclear. Further modifications in the C-terminal sequence of OT-BC are necessary to determine whether this moiety contributes to the high uterine receptor affinity of the bicyclic antagonists. In addition, the present 3D model does not specify the putative receptor-bound conformations for the Tyr[2] and Asn[5] side chains. Both NMR data and MD simulations suggest considerable conformational mobility of these side chains in solution. A systematic substitution of these residues with topographically constrained analogues[55] may reveal the side chain conformations recognized by the OT receptor and will contribute in development of more exact model for the receptor-bound conformations of OT antagonists. The proposed solution structure of OT-BC presents a good template for such conformationally directed modifications and for *de novo* design of peptide and non-peptide antagonists of oxytocin.

Acknowledgment. This work was supported in part by the U.S. Public Health Service Grant No. DK-17420. Dr. Katalin E. Kövér thanks the Hungarian Academy of Science for partial support through Grants OTKA T-014982 and OTKA D-23749.

Supporting Information Available: The experimental parameters used in NMR measurements, *z*-filtered TOCSY spectrum of [dPen[1]]OT-BC in DMSO-d_6, and table of torsional angles for representative low-energy conformations of analogues **1** and **2** (3 pages). See any current masthead page for ordering and Internet access instructions.

JA963736Y

(54) Shenderovich, M. D.; Hruby, V. J. Unpublished results. Details of molecular modeling of L-366,509 and its fitting to OT-BC analogues will be published elsewhere.

(55) (a) Hruby, V. J.; Al-Obeidi, F.; Kazmierski, W. *Biochem. J.* **1990**, *268*, 249−262. (b) Hruby, V. J. *Biopolymers* **1993**, *33*, 1073−1082 and references therein.